stacked lamellae.

From the in-situ SAXS patterns alone, it is clear that the lamellar thickness increases to twice the initial value on heating, but no conclusion on the mechanism involved during thickening could be made. It may occur either via interchain diffusion between the neighbouring crystals [9] or via an increase in the amount of amorphous material in between the crystalline core [10] (*i.e.* premelting of selective small lamellae within the lamellar stacks or surface melting of the crystals) or via a melting and recrystallisation process [11]. All these mechanisms would lead to development of the SAXS pattern as observed here. To investigate the mechanism involved during chain rearrangement in the crystalline core, we performed in-situ LA Raman mode experiments at *elevated temperatures*. As stated earlier, with the help of this technique one may follow the chain motion within the crystalline core. Before application of this technique for our experimentation, it is important to investigate the influence of temperature on the LA Raman mode in general. This has been performed in detail elsewhere (Rastogi *et al* 1997, in press), a summary of the results is given below.

So far, there has not been much effort to use the LA Raman mode as a tool to reveal chain arrangement in detail at temperatures higher than room temperature. Since the SAXS pattern does not show any substantial shift after annealing the solution-crystallised film before melting, we made use of such an annealed film to investigate the shift involved in LA Raman mode due to temperature. The LA Raman peak at 13.2cm^{-1} as shown in figure 5 at 25°C, which in fact is half the value for the LA Raman peak for lamellae having a thickness of 12nm, corresponds to a lamellar thickness of 24nm. No shift in the 13.2cm^{-1} band with increase in temperature up to 135°C is observed. It may be noticed that on heating below the melting temperature the peak position does not shift, nor does the peak broaden. Close to the melting temperature, a drop in the intensity with an asymmetric broadening of the LA Raman peak towards higher frequencies occurs. The following three conclusions can be drawn from these results. First, the absence of a peak shift in the peak below the melting temperature suggests that the length of the chain segments in the crystalline core of the annealed solution-crystallised film does not vary with temperature. Secondly, the LA Raman mode in the solution-crystallised film is not influenced by the temperature. Thirdly, close to the melting temperature, 138°C, a drop in the intensity with broadening of the peak to higher frequencies (*i.e.* decrease in thickness of the crystalline core) highlights the melting behaviour of the crystalline core. The shift to lower angles in the SAXS just before the melting temperature, shown as region CD in figure 3, can therefore be associated with the melting of the crystalline core, *i.e.*, the lamellar surface, rather than interchain diffusion between the adjacent lamellae. Taking into consideration the conclusions drawn from figure 5 we will analyse our experimental observations made on the unannealed solution-crystallised film during heating as shown in figure 6 and discussed below.

Figure 6a shows a set of collected LA Raman modes at different temperatures, displayed in two dimensions. The absence of a peak shift as a function of temperature in the annealed solution-crystallised film (figure 5) indicates that the shift in the LA Raman peak in figure 6a is solely due to chain rearrangement. Figure 6a shows a sharp peak at 26.7cm^{-1} at the start of the experiment, which broadens and moves to lower frequencies above the threshold temperature of 110°C. The peak shifts gradually from 26.7cm^{-1} to 13.2cm^{-1} with increasing temperature. The maximum shift to 13.2cm^{-1} is observed at ~130°C where the peak strengthens in intensity. On cooling, from 130°C to room

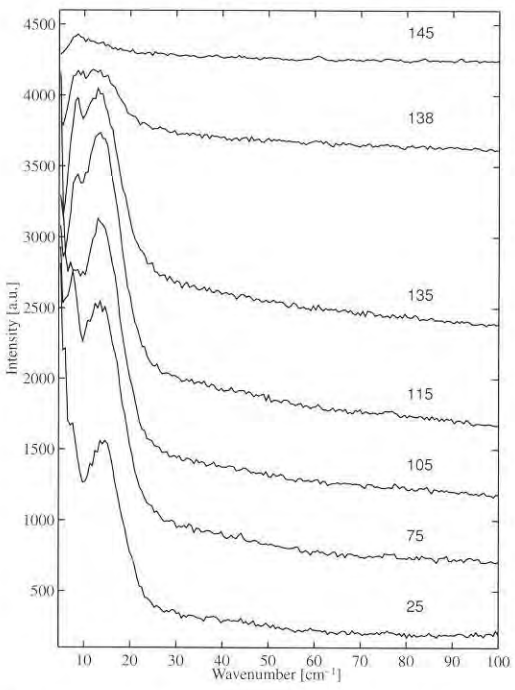

Figure 5: 2-D plot of the Longitudinal Acoustic (LA) Raman mode obtained during a heating scan from 50 to 135°C at 5°C/min of an annealed solution-crystallised film. The temperatures are indicated at the right of the figure.

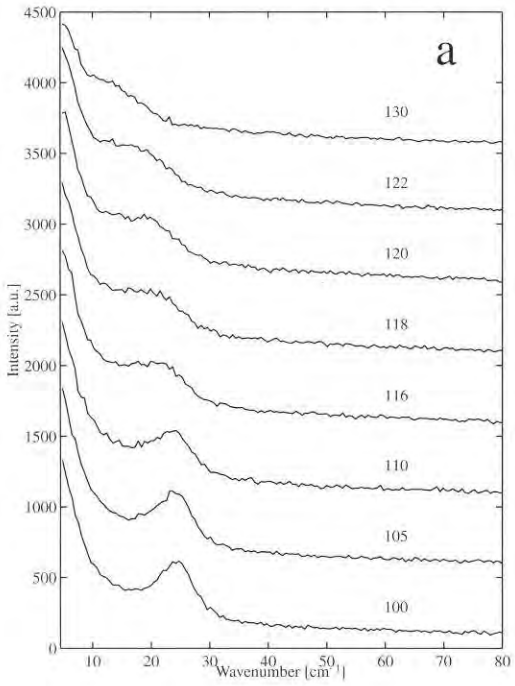

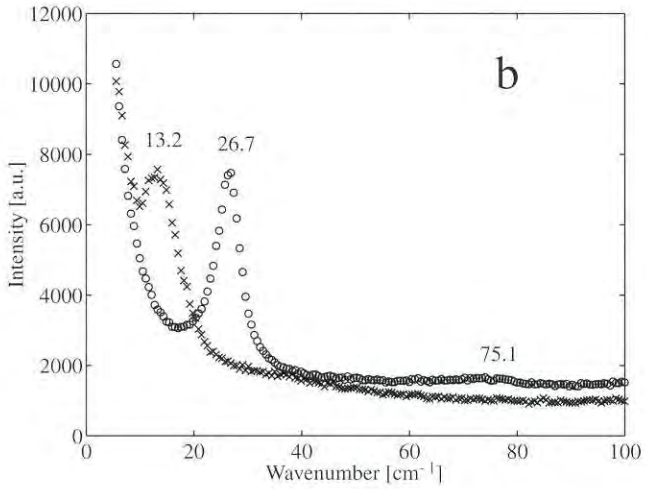

Figure 6: (a) 2-D plot of representative temperatures during heating scans (b) Comparison of the LA mode measured at room temperature between an unannealed and annealed film. (circles represent the unannealed film and crosses represent the annealed film)

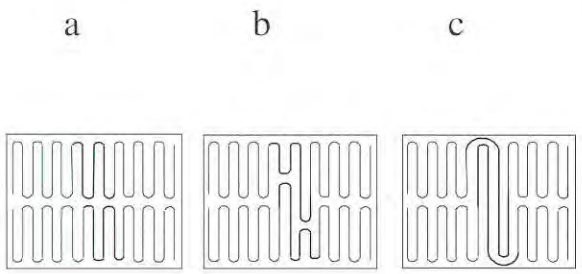

Figure 7: A schematic model to explain the doubling phenomenon in the regularly stacked adjacent lamellae. The bold line represents the test chain.

temperature, the band at 13.2cm^{-1} strengthens in intensity and becomes more distinct, as shown in figure 6b, which also shows a comparison with the unannealed film at room temperature. From the set of experiments shown in figures 5 and 6, it is clear that the crystalline core increases in thickness above the threshold temperature of 110°C to twice the initial value. The continuous shift in the LA Raman peak to lower frequencies cannot be associated with the melting of alternate lamellae or the crystalline core.

Therefore, the continuous shift in the LA Raman peak to lower frequencies clearly points to the fact that the increase in lamellar thickness is due to interchain diffusion between the regularly stacked adjacent lamellae - a situation realised in the solution -crystallised UHMW-PE films. Conversely, in the melt-crystallised polyethylene, the lamellae are arranged in spherulites and the lamellar thickness is widely distributed. Therefore the chain sliding diffusion leading to lamellar thickening cannot be realised.

The quantum increase in lamellar thickness has been observed in sharp fractionated paraffins [12], low molecular weight poly(ethylene oxide) [13,14], block copolymers (poly(ethylene oxide) and polystyrene) [15] and single crystals of nylon 6,6 [9]. The quantum increase in the thickening during the very initial stages of crystallisation in the sharp fractionated polyethylene from the melt has also been reported. One of the common morphological features, wherever the quantum increase in lamellar thickness is observed during annealing or heating below the melting temperature, is that the bulk of the material contains regularly stacked lamellae. A comparison between paraffins and UHMW-PE shows that the quantum increase in the thickening process is independent of molecular weight. This suggests that the mutual chain rearrangement between the adjacent crystals is a co-operative phenomenon where certain localised chain segments are involved, rather than the whole chain. Dislocations thus generated during thickening tend to move out of the crystal lattice to minimise the energy. A doubling scheme for the chain rearrangement between the adjacent crystals leading to doubling of the fold length has been proposed by Dreyfuss and Keller for nylon 6,6 [9] and thereafter proposed to occur by Barham and Keller [16] for the case of isothermal crystallisation of polyethylene, *i.e.*, primary thickening. With the help of neutron scattering, Sadler investigated the dimensions of

individual molecules and changes in relative positions of different molecules during the annealing of solution-grown single crystals of polyethylene. On following the chain trajectory of the deuterated molecule, it was found that on annealing at 123°C or lower the dimensions along the normal to the crystal lamellae increase in line with the lamellar thickness. During the thickening process the dimensions in the plane of crystallites were found to remain constant.

Taking the literature and our own results into account, the following model is proposed for the quantum increase in the lamellar thickness. The mechanism of the doubling process will be explained in view of the experimental details.

Figure 7a shows a schematic drawing of the regularly stacked lamellae as interpreted from the TEM of the solution-crystallised film (Figure 2a). Once the film is heated above the a-relaxation temperature, the thermodynamic driving force for lamellar thickening, necessary to minimise the surface free energy, will cause the chains to slide within the lamellae. The sliding chain within one lamella will push the chain in the adjacent lamella, as shown schematically by the bold line, representing the test chain, in figure 7b. For the sake of simplicity we have restricted ourselves to the selected region of the crystals. It has to be noted that the chains will slide between the adjacent crystals along the crystal lattice. Defects, associated with the fold surface which are introduced within the crystal lattice during chain sliding, will be removed once the crystal thickness has increased to twice the initial thickness. This is shown in figure 7c.

From figure 7c, it is evident that, once the lamellae have doubled to twice the initial value, chains get mutually entangled at the surface and further thickening via mutual chain rearrangement between the adjacent crystals can not occur. A further increase in lamellar thickness, which is logarithmic with time, should occur via melting and a recrystallisation process. In this respect our model is rather different than the one proposed by Keller and co-workers [9,16] in which thickening can occur in quantum jumps, not only giving doubling but also up to quadrupling.

Conclusions

From the above set of experiments the following conclusions could be drawn:

1. In the regularly stacked polyethylene single crystals, thickening occurs during annealing via a mutual chain rearrangement between the adjacent crystals which leads (ultimately) to a quantum increase, *i.e.*, doubling, of the lamellar thickness. The quantum increase in the lamellar thickness can be explained by our proposed model.

2. After the doubling process has been completed, further thickening via mutual chain rearrangement is hindered due to the fact that chains at the surface get entangled and, moreover, the regular stacking of lamellar crystals is lost. Further thickening of the doubled lamellar crystals involves a process of surface melting [10] or melting and recrystallisation [11].

3. The rate of increase in the lamellar thickness, ultimately leading to the quantum increase, will be dependent on the annealing temperature, *i.e.*, at higher temperatures, the doubling process will be faster.

Acknowledgement

The authors are grateful for the availability of the facilities at Station 8.2 of the Synchrotron Radiation Source (SRS), Daresbury, UK, and at Beamline ID-11/BL-2 of the European Synchrotron Radiation Facility (ESRF), Grenoble, France. Further, the authors are thankful for the experimental facilities available at Dilor, Lille, France for the Raman measurements.

References

[1] De Gennes, P.G. *Scaling Concepts in Polymer Physics*; Cornell Univ. Press, 1978.
[2] De Gennes, P.G. *J. Chem. Phys.* 1971, **55**, 572
[3] Doi, M., Edwards, S.F. *J. Chem. Faraday Trans.* 1978, **2**, 74, 1789, 1802, 1818
[4] Bastiaansen, C.W.M., Meijer, H.E.H., Lemstra, P.J. *Polymer* 1990, **31**, 1435
[5] Bastiaansen, C.W.M. *Ph.D. Thesis*; Eindhoven University of Technology, 1991.
[6] Ferry J.D. *Viscoelastic Properties of Polymers*, 2nd Ed., Wiley: New York, 1970.
[7] Bras, W., Derbyshire, G.E., Ryan, A.J., Mant, G.R., Felton, A., Lewis, R.A., Hall, C.J., Greaves, G.N. *Nucl. Instr. Meth. Phys. Rev. A* 1993, **A326**, 587
[8] Schaufele, R.F., Schimanouchi, T. *J. Chem. Phys.* 1967, **47**, 3605

[9] Dreyfuss, P., Keller, A. *J. Macromol. Sci.-Phys.* 1970, **B4**(4), 811
[10] Fischer, E.W. *Pure Applied Chem* 1972, **31**, 113
[11] Mandelkern, L. *Macromol.* 1969, **2**, 644
[12] Ungar, G., Stejny, J., Keller, A., Bidd, I., Whiting, I.C. *Science* 1985, **229**, 386
[13] Kovacs, A.J., Straupe, C. *Faraday Disc. Chem. Soc.* 1979, **68**, 225
[14] Cheng, S.Z.D., Chen, J. *J. Polym. Sci. B Polym. Phys.* 1991, **29**, 311
[15] Ryan, A.J., *et al.* Manuscript in preparation.
[16] Barham, P.J., Keller, A. *J. Polym. Sci. B Polym. Phys.* 1989, **27**, 1029
[17] Sadler, D.M. *Polymer Comm.* 1985, **26**, 204

X-PLOR for Polycrystalline Fibre Diffraction

R.C.Denny[1,2], M.Shotton[3] and V.T.Forsyth[3]

1 Biophysics Section, Blackett Laboratory, Imperial College, London SW7 2BZ
2 CLRC Daresbury Laboratory, Warrington WA4 4AD.
3 Physics Department, Keele University, Keele, Staffordshire ST5 5BG

Introduction

X-PLOR is a flexible software package for molecular dynamics, protein crystallography and NMR [1]. Among other things, the X-PLOR system allows a chosen target function to be used as an empirical X-ray energy term which can be added to the potential energy of a macromolecule. The techniques of energy minimization and simulated annealing can then be applied to the molecule to ensure reasonable stereochemistry and an optimal fit to the data. X-PLOR version 3.1 has certain limitations as far as fibre diffraction is concerned:

i) It is not possible to connect the asymmetric units of crystallographic or strict non-crystallographic symmetry together with covalent bonds.
ii) The diffraction data are treated as independent structure factors and cannot be input as composite intensities or overlapping Bessel function contributions.

A modified version of X-PLOR has addressed these problems for the case of structures with strict helical symmetry and continuous layer line intensity data and has already proved extremely useful in the study of filamentous viruses [2]. Once X-PLOR 3.1 has been installed, these new and modified routines comprising FX-PLOR can be built into the system very easily. See ***http://www.molbio.vanderbilt.edu/fibre/software.html.*** The purpose of this work is to build upon FX-PLOR to provide a system suitable for both non-crystalline and polycrystalline fibres. Two examples are given below which demonstrate the power and flexibility of FX-PLOR using simulated fibre diffraction data.

Modifications

In systems that give rise to fibre diffraction, molecules often span more than one asymmetric unit. For a molecule consisting of a simple chain of atoms this would involve defining an extra bond, two extra bond angles and three extra torsion angles to connect asymmetric units above and below the one in which the atomic coordinates of the molecule are defined. The symmetry linkage routines supplied with FX-PLOR cater for molecules where strict non-crystallographic (helical) symmetry applies. Polycrystalline fibre samples are more likely to have approximate helical symmetry and strict crystallographic symmetry. Therefore, the symmetry linkage routines in FX-PLOR required modification to allow the use of crystallographic symmetry and translations along a unit cell edge vector. This means that a continuous chain can be built passing from asymmetric unit to asymmetric unit or through the bottom and top of the unit cell.

Some of the crystallographic target functions available in X-PLOR have been adapted for polycrystalline fibre diffraction. The *F2F2* and *E2E2* target functions can be used with some modification to take account of reflection overlap. The *RESIDUAL* option has been more extensively modified to scale observed and calculated intensities together rather than structure factor moduli and to treat composite diffraction spots. These functions have been redefined for the case of a polycrystalline fibre as follows:

$$F2F2 = 1 - CC\left(\left\{w_{hkl} I^{obs}_{hkl}\right\}, \left\{w_{hkl} \sum_{h'k'l' \in M(hkl)} m_{h'k'l'} I^{cal}_{h'k'l'}\right\}\right) \quad (1)$$

$$E2E2 = 1 - CC\left(\left\{\frac{w_{hkl} I^{obs}_{hkl}}{\left\langle w_{hkl} I^{obs}_{hkl}\right\rangle_{bin}}\right\}, \left\{\frac{w_{hkl} \sum_{h'k'l' \in M(hkl)} m_{h'k'l'} I^{cal}_{h'k'l'}}{\left\langle w_{hkl} \sum_{h'k'l' \in M(hkl)} m_{h'k'l'} I^{cal}_{h'k'l'}\right\rangle_{bin}}\right\}\right) \quad (2)$$

where $M(hkl)$ is the set of indices belonging to a composite diffraction spot indexed as hkl, $m_{h'k'l'}$ is the multiplicity factor of reflection $h'k'l'$ and w_{hkl} is the weight to be applied to the observation. CC is the correlation coefficient defined,

$$CC(X,Y) = \frac{\langle (x - \langle x \rangle)(y - \langle y \rangle) \rangle}{\sqrt{\langle (x - \langle x \rangle)^2 \rangle \langle (y - \langle y \rangle)^2 \rangle}} \forall x \in X, y \in Y \quad (3)$$

The *RESIDUAL* function is now given by,

$$RESIDUAL = \sum_{hkl} w_{hkl} \left(I_{hkl}^{obs} - k \sum_{h'k'l' \in M(hkl)} m_{h'k'l'} I_{h'k'l'}^{cal} \right)^2 \quad (4)$$

where the scale factor k is the least-squares solution for scaling intensities,

$$k = \frac{\sum_{hkl} w_{hkl} I_{hkl}^{obs} \sum_{h'k'l' \in M(hkl)} m_{h'k'l'} I_{h'k'l'}^{cal}}{\sum_{hkl} w_{hkl} \left(\sum_{h'k'l' \in M(hkl)} m_{h'k'l'} I_{h'k'l'}^{cal} \right)^2} \quad (5)$$

Where the term "R-factor" is used in the text it refers to the quantity,

$$R = \frac{\sum_{hkl} w_{hkl} \left| I_{hkl}^{obs} - k \sum_{h'k'l' \in M(hkl)} m_{h'k'l'} I_{h'k'l'}^{cal} \right|}{\sum_{hkl} w_{hkl} I_{hkl}^{obs}} \quad (6)$$

Example 1: Refinement of a Perturbed Structure

Data and Model Preparation

A model structure of the D form of poly d(A-T).poly d(A-T) similar to that of Arnott *et al*, [3], was placed in a P1 unit cell with dimensions a = b = 17.2Å, c= 24.1Å, $\alpha = \beta = 90°$, $\gamma = 94.5°$. These cell dimensions provide approximately a quarter of the number of unique measurements for fibre diffraction (471 diffraction spots) than for single-crystal data (1843 reflections) between 10Å and 2Å resolution. This choice of cell and alternative descriptions have been reported by Forsyth *et al*, [4]. The model was energy minimized without X-ray or packing terms and a set of structure factors were calculated. These structure factors were saved to be used as simulated data for subsequent trials. The structure was then subject to a molecular dynamics simulation at 500K for 0.5ps followed by a final round of energy minimization in order to produce a perturbed model as a starting point for refinement. The simulated data were used to provide two sets of input: one in which all reflections were treated as independent observations (SC dataset) and one in which systematic overlaps and some close lying reflections due to cylindrical averaging were processed to produce a composite observation (PF dataset).

Energy Minimization and Simulated Annealing

The first test was to compare the results of energy minimization (EM) when the X-ray energy term was included with the single-crystal dataset and the polycrystal dataset. Separate trials were run with the *F2F2* target function and the *RESIDUAL* target function. A necessary initial stage is to determine the weight with which the X-ray energy is to added to the other energy terms. This was done using the method suggested by Brünger *et al* [5], where a short molecular dynamics simulation is performed on the initial model and the energy gradient at the end of the simulation is compared with the X-ray energy gradient. The weight of the X-ray energy is then chosen so as to make the gradients equal. Clearly, the subsequent use of a different target function requires that the weight be recalculated. Each observation was assigned unit weight. A maximum of 120 cycles was allowed for each refinement.

The same weight determined for the X-ray energy for energy minimization is appropriate for simulated annealing (SA). An initial energy minimization must be performed before SA can begin to decrease any large energy gradients in the initial model. At each temperature stage in the cooling schedule, a molecular dynamics simulation was run for 0.025ps. The temperature was then reduced by an increment (25K) and the process repeated until the temperature had reached 300K. An EM refinement, with an identical protocol to the one described above, was performed when the final temperature had been reached.

Results

Both the *F2F2* and the *RESIDUAL* target functions were employed in the EM trials. The rms deviation in atomic position was calculated between both the final models achieved by the refinements and the perturbed starting model (Δs) and between the refined models and the test model used to calculate the simulated data (Δt). The rms deviation between the test model and the starting model was 1.32Å. The results of the EM trials are summarized in table 1.

Data	Target	*R* start	*R* end	*CC* start	*CC* end	Δt	Δs
SC	*F2F2*	0.752	0.170	0.629	0.989	0.334	1.345
PF	*F2F2*	0.589	0.448	0.774	0.913	1.259	0.633
SC	*RESI*	0.752	0.157	0.629	0.991	0.296	1.295
PF	*RESI*	0.589	0.157	0.774	0.991	0.678	1.051

Table 1: The results of the energy minimization trials for the single-crystal (SC) and polycrystalline fibre (PF) datasets are shown. Start and end R-factors and correlation coefficients are given along with rms deviations in atomic position. Δs refers to the deviation between the perturbed starting model and the final model achieved in the refinement and Δt refers to the deviation between the fianl model and the test model.

Data	T start	*CC* end	*R* end	Δt	Δs
SC	4000	1.000	0.009	0.230	1.333
PF	4000	1.000	0.025	0.339	1.351

Table 2: The results of the simulated annealing trials are shown. T start refers to the initial temperature of the annealing schedule, other meanings are as for table 1.

The results for the SC data with the *F2F2* and the *RESIDUAL* target functions are similar, perhaps slightly favouring the use of the *RESIDUAL* function. The EM method was slightly less effective in the PF case, achieving some progress in 77 cycles of the minimization procedure with the *F2F2* target before the search was abandoned. Refinement of the PF data with the *RESIDUAL* target gave an identical R-factor and *CC* as in the SC case. However, the final rms deviation from the test model was slightly greater than for the SC case.

Only the *RESIDUAL* target was used for the SA trials on the basis that this target had allowed greater progress in the EM trials for the PF data. The results of these trials are summarized in table 2. Clearly, the result of the both trials show the efficacy of the method with an appropriate target function and annealing schedule.

Example 2: Comparison of a Self-Rotation Search with a Rotation Search using a Perturbed Model

Data and Model Preparation

A test model and perturbed model were prepared in a similar way to that used in example 1, except that $P2_1$ symmetry was imposed on the structures. A PF dataset was calculated from the test model with a resolution range of 25-2Å which was used as data in the subsequent rotation searches.

Rotation Searches

It is a simple task to set up a loop in the X-PLOR language to rotate the atomic coordinates by some angular increment about a specified axis. It is then possible to monitor the R-factor as a function of resolution for each rotation. Two searches were performed, both over 180° at 5° increments, one being a self-rotation search using the test model coordinates and the other being a cross-rotation search using the perturbed model coordinates.

Results

The self-rotation search shows the maximum R-factor that can be achieved by a simple rotation of the atomic coordinates in the unit cell. The results of this search are shown in figure 1(a): the R-factors are shown for resolution ranges 25.0-2.0Å, 25.0-4.0Å and 2.09-2.0Å. It is clear that the 25.0-.4.0Å R-factor shows the greatest contrast between molecular orientations. The four-fold helical symmetry of the test model and the closeness of the cell to being tetragonal is shown by the near perfect repetition of the curves at 90° intervals. Deviations from this repeat are most easily discernible in the 2.09-2.0Å curve.

The rms deviation in atomic coordinates between the test model and the perturbed model was 0.91Å and the corresponding R-factor (at 0° rotation) was 0.587 using the full resolution range. Figure 1(b) shows the results of the cross-rotation search. Again, the 25.0-4.0Å R-factor shows the greatest contrast with molecular orientation while the 2.09-2.0Å R-factor

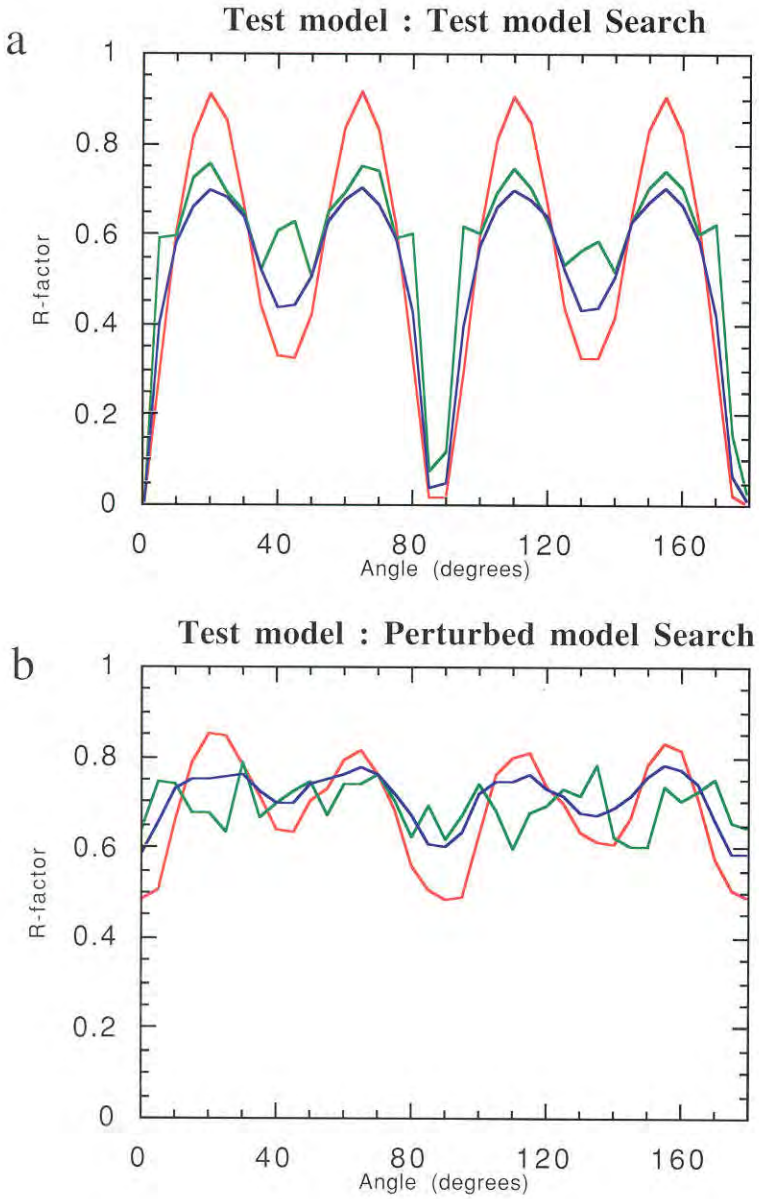

Figure 1: This shows the results of the rotation searches. R-factors are shown for data in three resolution ranges: 25-4Å (red), 25-2Å (blue), 2.09-2Å (green). Graph (a) shows the R-factor curves for the self-rotation search for the test model, graph (b) shows the curves for the cross-rotation search between the test model and the perturbed model.

indicates very little correlation to the low resolution curve or to the corresponding self-rotation curve.

Conclusions

X-PLOR provides a very flexible language for performing calculations using atomic coordinates and X-ray diffraction data. The extension of this package to cope with fibre diffraction applications should enable researchers to identify more rapidly a strategy suited to dealing with their data processing requirements.

Pannu & Read [6] have implemented two maximum likelihood target functions in X-PLOR, increasing the radius of convergence of refinement. Bricogne [7] has formulated a likelihood function for overlapping intensity data. Implementation of this function within FX-PLOR may prove helpful where there is a significant amount of diffracting material in the unit cell not represented in the model.

References

[1] Brünger, A.T., Kuriyan, J & Karplus, M. (1987). *Science* **235**, 458-460

[2] Wang, H. & Stubbs, G (1993) *Acta Cryst.* **A49,** 504-513

[3] Arnott, S., Chandrasekaran, R., Puigjaner, L.C., Walker, J.K., Hall, I.H., Birdsall, D.L. & Ratliff, R.L. (1983). *Nucleic Acids Research* **11**, 1457-1474

[4] Forsyth, V.T., Mahendrasingam, A., Langan, P., Pigram, W.J., Stevens, E., Al-Hayalee, Y., Bellamy, K.A., Greenall, R.J., Mason, S.A. & Fuller, W. (1990). *Inst. Phys. Conf. Ser.* **101**, 237

[5] Brünger, A.T., Karplus, M. & Petsko, G.A. (1989). *Acta Cryst.* **A45**, 50-61

[6] Pannu, N.S. & Read, R.J. (1996). *Acta Cryst.* **A52**, 659-668

[7] Bricogne, G. (1991). *Acta Cryst.* **A47**, 803-829

Structure of the Capsid of Pf3 Inovirus Determined from 3.1 Å Fibre Diffraction Data

L.C.Welsh, M.F.Symmons, D.A.Marvin and R.N.Perham

Cambridge Centre for Molecular Recognition, Department of Biochemistry, University of Cambridge, 80 Tennis Court Road, Cambridge, CB2 1GA, U.K.

Many Inovirus (filamentous bacteriophage) virions have been isolated and all share certain structural and biological features. The virions are between 800 and 2000nm in length and about 6nm in diameter, depending on the biological strain. They comprise a semi-flexible helical tube of several thousand copies of a major coat protein subunit surrounding a core of single-stranded circular DNA. The major coat protein subunits of virions of different strains of Inovirus are largely alpha-helical, but have quite different amino-acid sequences. However, the sequences have a similar domain structure, with acidic residues near the N-terminus, a continuous stretch of about 20 apolar residues near the centre of the sequence, and a collection of basic residues near the C-terminus. The N-termini of the major coat protein subunits are on the outside of the capsid and the C-termini are on the inside where they interact with the viral DNA. The virions are held together by hydrophobic interactions between the apolar domains of neighbouring subunits. The virions infect Gram-negative bacteria and are extruded through the bacterial membrane during the subsequent virion assembly process.

Two Inovirus capsid helical symmetry classes have been identified from fibre diffraction patterns: class I includes strain fd; class II includes strain Pf1. Pf1 virions undergo a reversible temperature-induced phase transition at about 10°C between a higher (Pf1H) and a lower (Pf1L) temperature helical symmetry form . Very well-resolved fibre diffraction patterns from Pf1 at temperatures below 10°C enabled many Bessel-function terms that overlap in the higher temperature form diffraction pattern to be separated. Accurate intensity measurements for native and heavy-atom derivatives therefore resulted in a diffraction data set as extensive as a single crystal diffraction data set at the same resolution (4.0Å in R and 2.5Å in Z). These data enabled precise atomic models to be built for the Pf1 major coat protein [1]. Models of class I virions have been built from these that are consistent with the much more limited fibre diffraction data available from class I virions [2].

Pf3 Inovirus has a particularly intriguing structural feature: the Pf3 major coat protein has two basic residues near the C-terminus, like Pf1, but has more than twice as much DNA per unit length. Knowledge of the virion structure is essential for an understanding of the assembly process, the infection process, and DNA/protein interactions within the virion. Similarities and differences between strains help to define the essential aspects of these processes. Therefore, we recorded high resolution X-ray fibre diffraction data from Pf3 and used these data to determine the structure and interactions of the major coat protein subunit within the virion.

X-ray diffraction data recorded from magnetically aligned fibres of virions of the Pf3 strain of Inovirus show that the Pf3 capsid has the same, class II, helical symmetry as that of the higher temperature form of the Pf1 virion. A quantitative comparison of the integrated layer-line intensities extracted from Pf3 (Figure 1) and Pf1 diffraction patterns, using CCP13 software, gives a correlation coefficient of 0.89, showing that the structures of the Pf3 and Pf1 capsids are very similar. However, Pf3 virions do not undergo a temperature-induced helical symmetry transition of the kind observed for Pf1 virions [3].

We have determined the structure of the Pf3 major coat protein within the capsid by a form of molecular replacement from a model of the major coat protein of the higher temperature form of Pf1. A 5Fo-4Fc Fourier synthesis electron density map of the Pf3 capsid was calculated from the Pf3 fibre diffraction amplitude data by separating overlapping Bessel function terms and taking phases from an all alpha-helix model of the Pf1 major coat protein, stripped of side-chains atoms. A set of initial atomic models of the Pf3 major coat protein covering a discrete range of azimuthal major coat protein subunit orientations within the capsid was built, consistent with both the observed fibre diffraction data and the initial Pf3 major coat protein electron density map.

We were able to discriminate between some of the models of the Pf3 capsid on the basis of the sequence

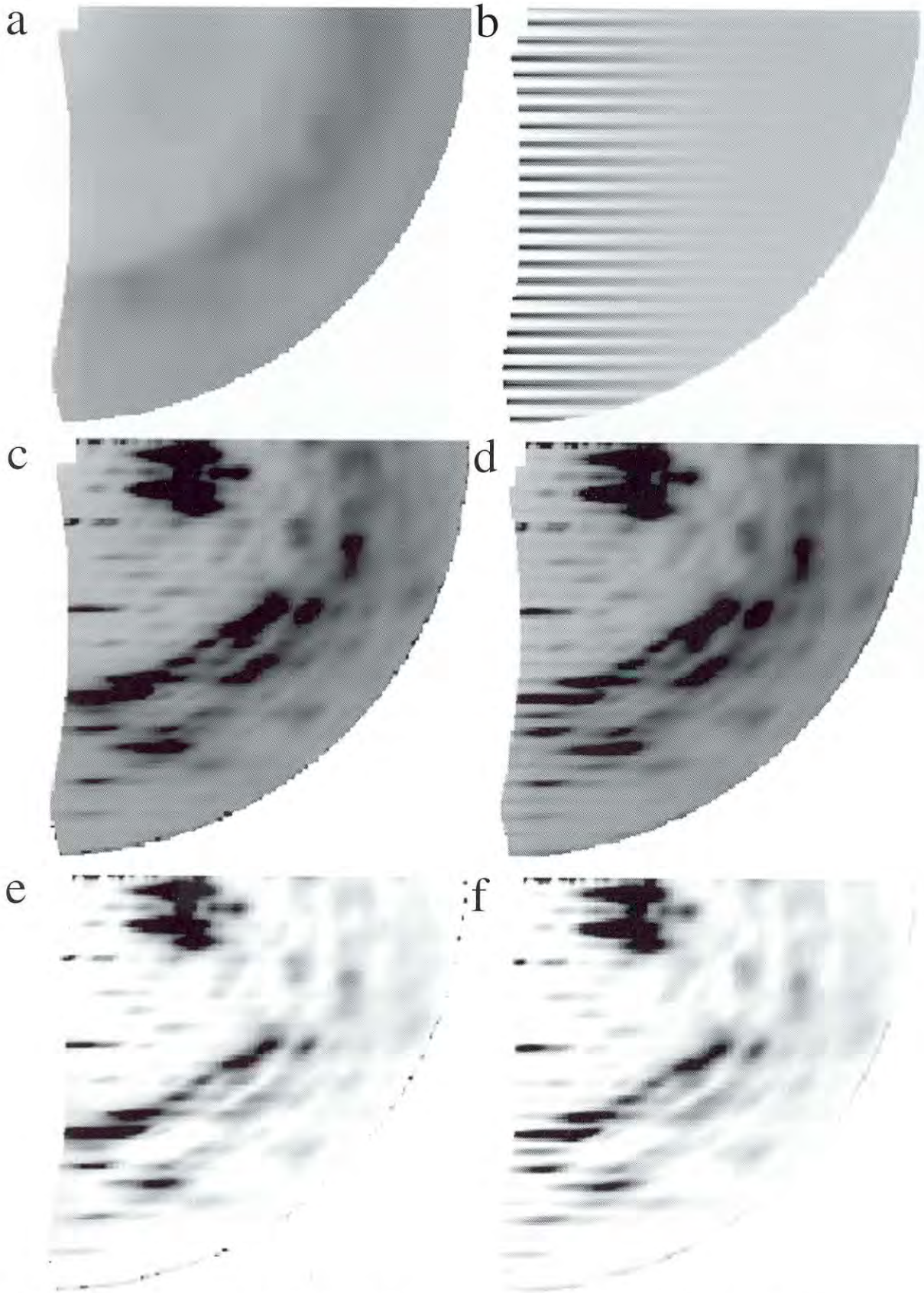

Figure 1: Stages in the processing of the Pf3 fibre diffraction pattern using CCP13 software. The diffraction pattern was recorded on a MAR image plate on station 7.2 of the SRS at CLRC Daresbury. The outer radius of is at 0.32Å^{-1}. The c repeat is 76.2Å. (a) The background scattering calculated from the experimental Pf3 diffraction pattern using the roving window method in the LSQINT program. (b) An image of the layer-line profiles [8] generated by LSQINT to fit the layer-line intensity distributions, before being fitted to the observed diffraction pattern. The disorientation is 2.0° and the coherence length is 200Å. (c) The observed diffraction pattern mapped into reciprocal space and quadrant averaged using the FTOREC program. (d) A simulated diffraction pattern using the integrated layer-line intensity distributions generated by LSQINT from the observed diffraction pattern in (c) and the background scattering shown in (a). (e) The observed diffraction pattern of (c) with the calculated background scattering of (a) subtracted. (f) The simulated diffraction pattern of (d) without the calculated background scattering. The R-factor calculated between the image and that shown in (e) is 0.21.

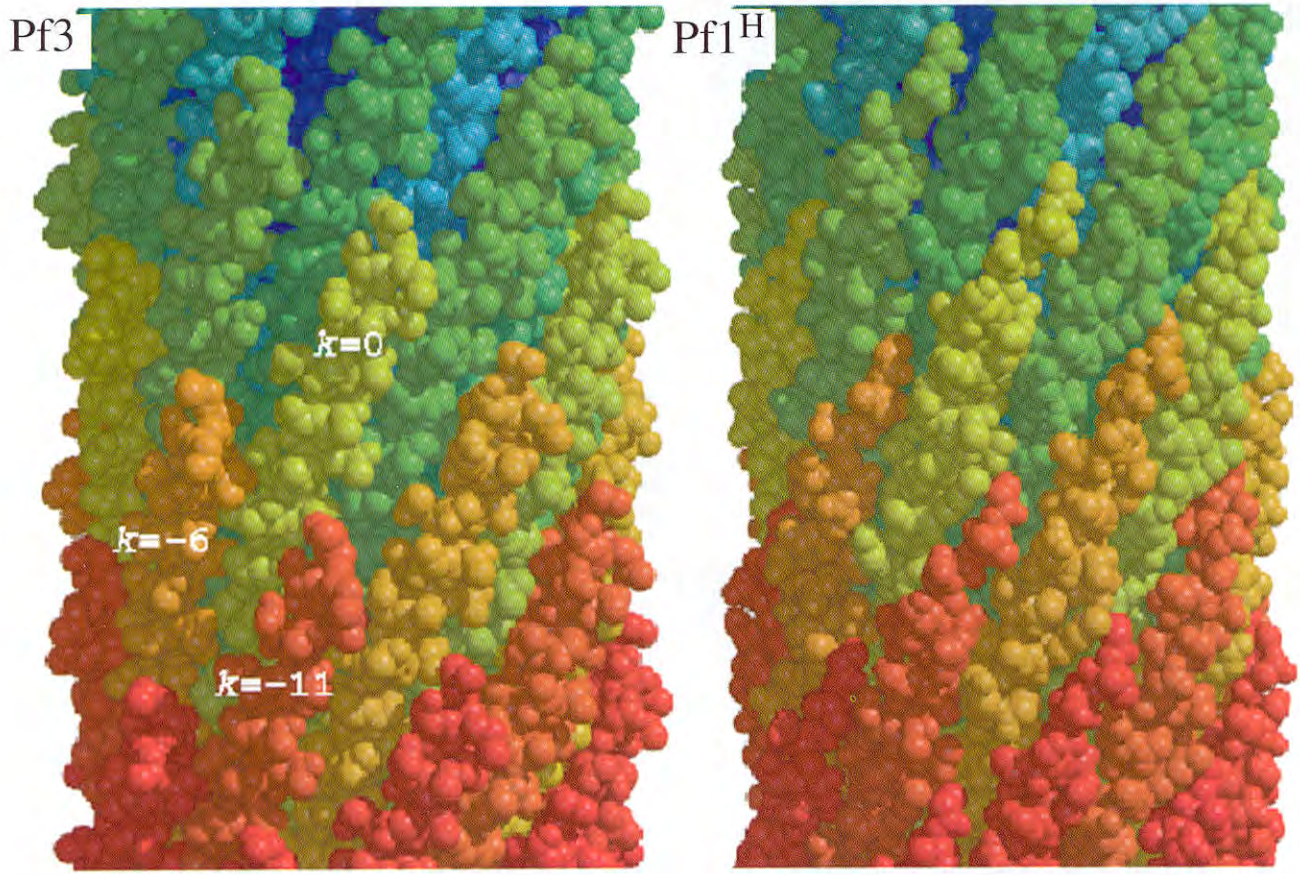

Figure 2: Space-filling representation of a 100Å long section of the final model of the Pf3 capsid and the current model of the higher temperature form of the Pf1 capsid. Side-view of the capsids, virion axis vertical, N-termini of the major coat protein subunits towards the top. The subunit indices of the nearest neighbours of a subunit arbitrarily indexed as 0 are shown.

homology resulting from the structural alignment of the Pf3 and Pf1 major coat protein sequences. Furthermore, the existence of a large number of well determined globular protein structures has led to the derivation of a number of empirical rules for validating models of protein structures and we used two such methods to help discriminate between the Pf3 models [4,5]. Three of the initial Pf3 models emerged from these tests as viable candidates for the structure of the Pf3 major coat protein in the capsid, but one model was clearly favoured over the others by these criteria and also by supplementary data from spectroscopic techniques. These three most likely Pf3 models were refined against the observed fibre diffraction data.

Both Cartesian co-ordinate and torsion angle coordinate simulated annealing refinement protocols were tested by simulation for model refinement against continuous transform fibre diffraction data of the kind obtained from Pf3 virions. Refinement using torsion angle dynamics reduces the number of degrees of freedom of the models [6], but was found to have a lower radius of convergence for Pf3 models refined against fibre diffraction data; models were therefore refined using Cartesian coordinate simulated annealing. In addition, model refinement against continuous transform fibre diffraction data using the free R-factor [7] was tested by simulation and found to be effective in detecting global errors in a model structure if multiple refinements were carried out, starting from different initial atomic velocities. In the refinement of the three potential Pf3 models against the experimental Pf3 diffraction data the free R-factor clearly indicated one of the models as being superior to the others. Encouragingly, this was the same model that was consistently favoured by the other criteria used to discriminate between the initial models earlier in the structure determination procedure. This model was taken as the best model of the structure of the Pf3 major coat protein in the capsid.

The model of the Pf3 capsid thus determined shows that the overall structure of the capsid is very similar to that of Pf1 (Figure 2). Both capsids possess similar networks of non-polar inter-subunit van der Waals contacts between side-chains of residues in the central regions of the major coat proteins. However, there are significant differences in the structures of the N and C-termini of the proteins (Figures 2 and 3). In particular the N-terminus of the Pf3 major coat

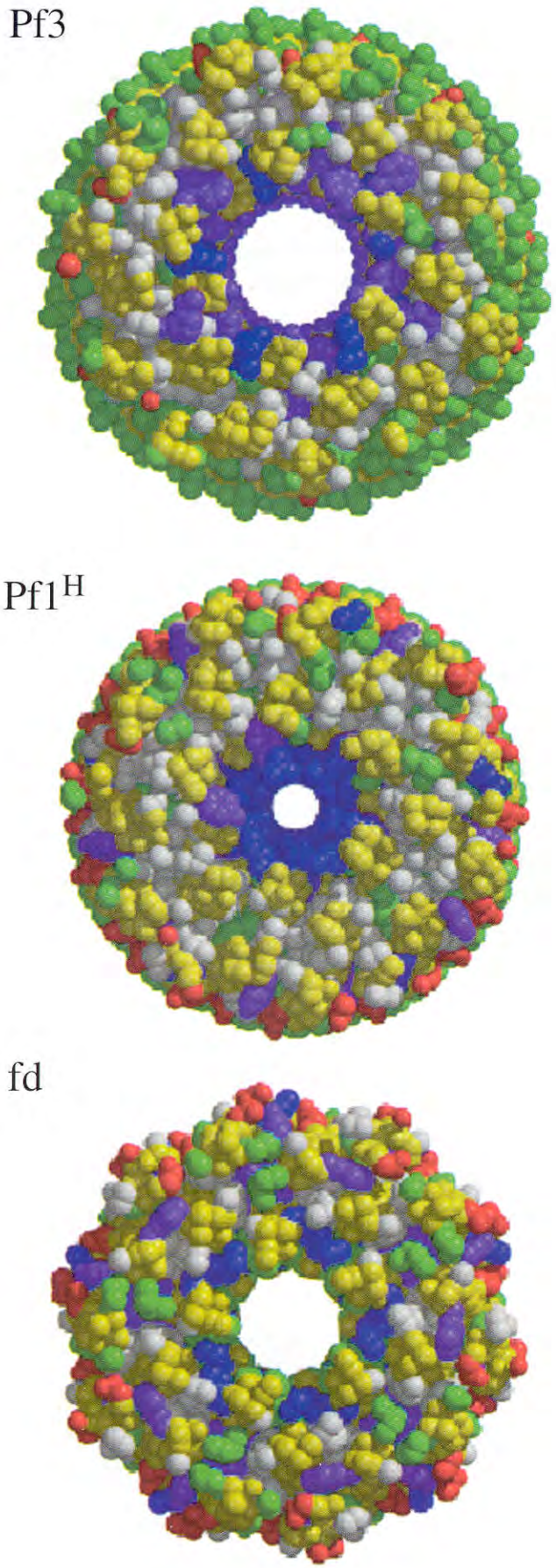

Figure 3: Space-filling representations of models of Inovirus capsids. View down the long axis of the capsids showing the central core occupied by the single-stranded circular DNA (for which there are currently no reliable atomic models). Backbone atoms are coloured yellow, acidic side-chains are coloured red, polar side-chains are coloured green, apolar side-chains are coloured white, aromatic side-chains are coloured purple, and basic side-chains are coloured blue. Models of the Pf3, Pf1H and the fd capsid. The average diameter of the Pf3 core is 25Å, that of fd is 22Å and both have about two and half times as much DNA per unit length as Pf1 which has an average diameter of about 10Å. The maximum radius of the Pf3 models is 33Å and that of the Pf1H models is 30Å, consistent with differences in the equatorial diffraction data from these strains. The maximum radius of the fd model is 31Å.

protein is in an alpha-helical conformation whereas the first five N-terminal residues of Pf1 are not [1]. The nature of the C-terminal region of the inner core of the model of the Pf3 capsid shows that there must be significant DNA/protein interactions in this virion involving both charged side-chains and aromatic side-chains, whereas the DNA/protein interactions in the models of the Pf1 and fd virions predominantly involve charged side-chains (Figure 3). This difference in DNA/protein interactions may result in differences in the low-frequency dynamics of the virions and thereby be responsible for the absence of a temperature transition in the Pf3 virion.

Acknowledgements

We are grateful to the Leverhulme Trust and the Wellcome Trust for support.

References

[1] Gonzalez, A., Nave, C., & Marvin D.A., (1995). *Acta Cryst.* **D51**, 792-804.
[2] Marvin, D.A., Hale, R.D., Nave, C. & Helmer-Citterich, M., (1994). *J. Mol. Biol.* **235**, 260-286.
[3] Marvin, D.A., Nave, C., Bansal, M., Hale, R.D. & Salje, E.K.H., (1992). *Phase Transit.* **39**, 45-80.
[4] Eisenberg, D. & McLachlan, A.D., (1986). *Nature* **319**, 199-203.
[5] Lüthy, R., Bowie, J.U. & Eisenberg, D., (1992). *Nature* **356**, 83-85.
[6] Brunger, A.T. & Rice, L.M., (1997) *Meth. Enzymol.* **277**, 243-269.
[7] Brunger, A.T., (1997) *Meth. Enzymol.* **277**, 366-396.
[8] Fraser, R.D.B., Macrae, T.P., Miller, A. & Rowlands, R., (1976) *J. Appl. Cryst.* **9**, 81-94.

Complex Phases in Block Copolymer Solutions

J.P.A.Fairclough[1], A.J.Ryan[1,2], C.Booth[3], H.Li[3], G-E.Yu[3], I.W.Hamley[4], J.A.Pople[4], K.Mortensen[5], K.Almdal[5], A.J.Gleeson[4].

1. Department of Chemistry, University of Sheffield, Sheffield, S3 7HF, UK
2. CLRC, Daresbury Laboratory, Daresbury, Cheshire, WA4 4AD, UK
3. Department of Chemistry, University of Manchester, Manchester M13 9PL, UK
4. School of Chemistry, University of Leeds, Leeds, LS2 9JT, UK
5. Risø National Laboratory, DK-4000, Roskilde, Denmark

Block copolymers are two or more chemically distinct polymers joined together. The simplest form of block copolymer is a diblock copolymer where the two polymers are joined at their ends. A triblock copolymer is shown in the diagram below.

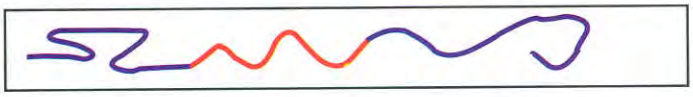

Figure 1: Schematic diagram of a triblock copolymer

As such this is the next stage of complexity from a diblock. If the polymers were not joined together by a covalent bond at their ends, then at low temperature they would macrophase separate, as fat and water do in milk over time. However, since they are joined together this is prevented and microphase separation occurs [1]. In the systems that we have studied one of the blocks, the blue one (poly(oxyethylene)) is hydrophilic and the middle block, the red one, (poly(oxybutylene)) is hydrophobic. Hence, if the triblock copolymer is added to water, the poly(oxyethylene) block is solvated in the water and

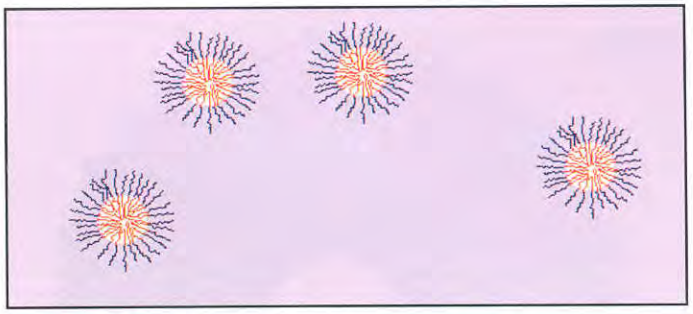

Figure 2: Micelles of EBE triblock copolymer in water.

the poly(oxybutylene) block tries to curl up to prevent contact with water. If there are sufficient other triblock copolymer molecules around then the best way this can be done is for the molecules to form small spheres called micelles, were the poly(oxybutylene) blocks are on the inside away from the water and the poly(oxyethylene) are on the outside.

As the concentration is raised, the micelles aggregate and form complex structures such as fcc or hcp cubic structures, hexagonal cylinders or lamella solutions [2]. The main point of all this is that the change in structure can be brought about by changing temperature instead of changing composition as the solvent quality changes with temperature. In addition the different structures have different rheology. Thus by changing the temperature the system can change from a stiff gel that does not flow to a mobile sol that does.

We have studied three block copolymer solutions by Synchrotron SAXS and SANS. They consisted of aqueous solutions of a triblock copolymer of poly(oxyethylene)-poly(oxybutylene)-poly(oxyethylene), commonly noted $E_nB_mE_n$. The three triblock copolymers $E_{16}B_{10}E_{16}$, $E_{20}B_{10}E_{20}$ and

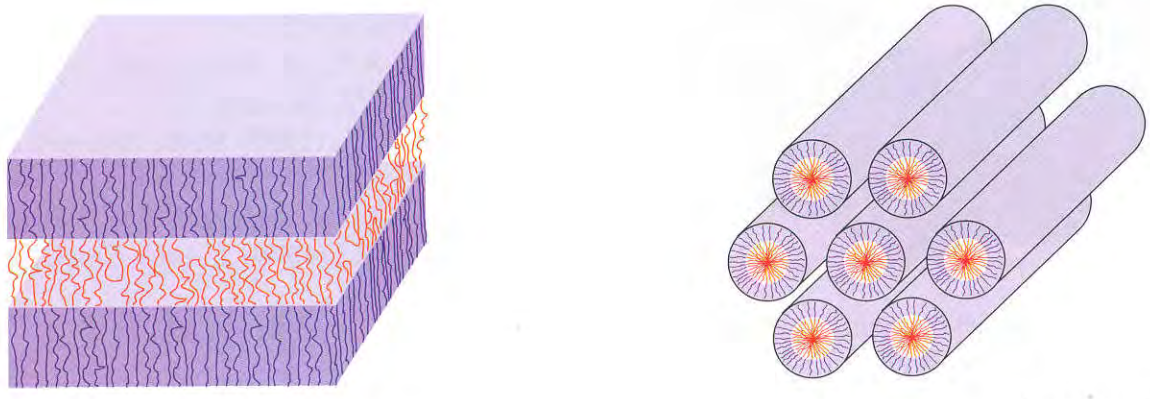

lamella **hexagonal**

Figure 3: Lamella and hexagonal cylinder structure in water. The water is excluded from the B block areas (red).

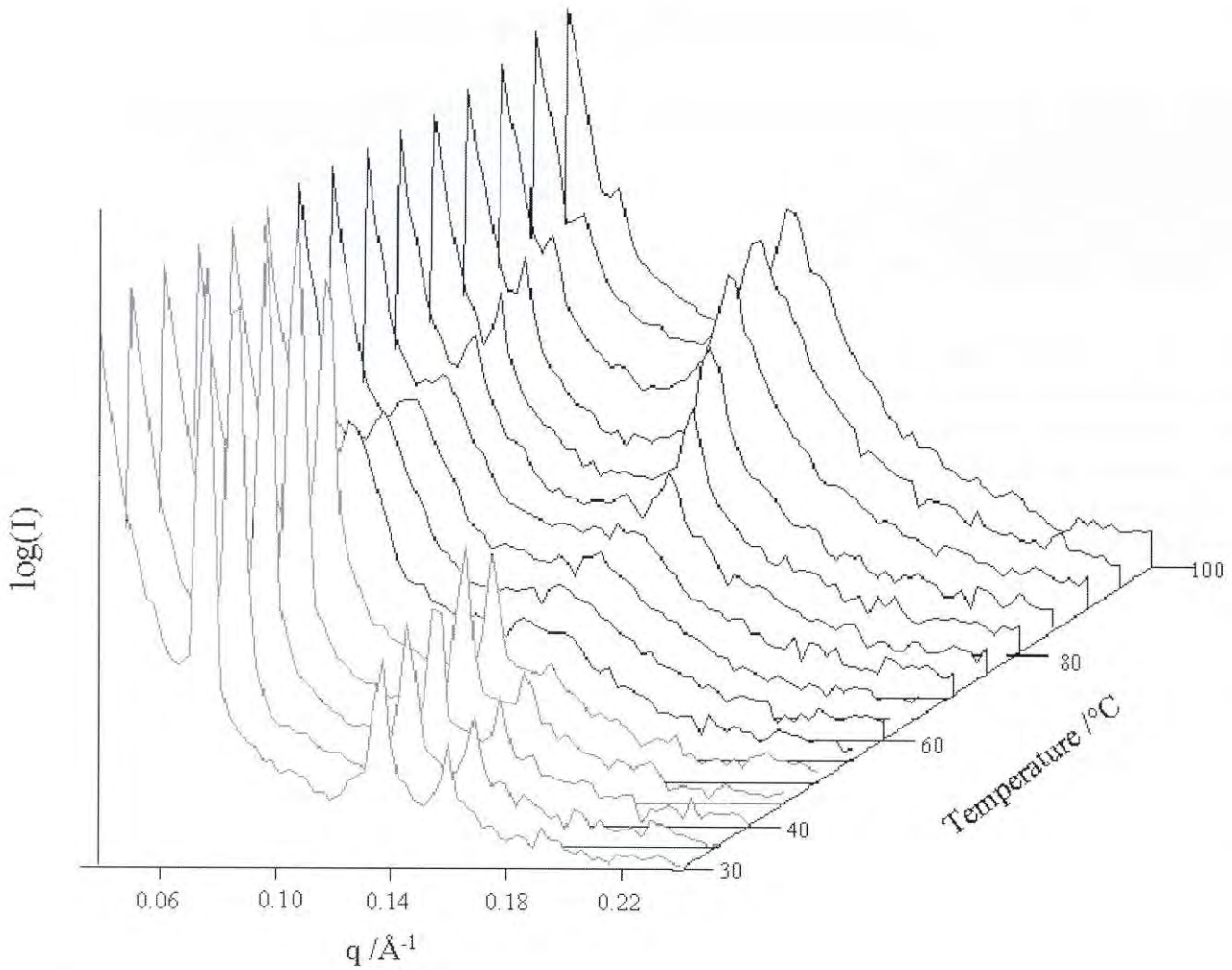

Figure 4: The SAXS patterns observed during a slow heating ramp for a 45wt%. $E_{16}B_{10}E_{16}$ in water. The transition from hexagonal cylinders through disorderd sol to lamella stacks can clearly be seen.

$E_{35}B_{10}E_{35}$ are readily soluble in water forming a range of phases at different compositions. It was the purpose of this study to determine the stable phases and to study their response to shear.

The initial stages of the experimental program were concerned with the temperature-morphology profile of the samples. The samples were placed in capillary tubes in a Linkam hotstage and studied by synchrotron SAXS on Station 8.2 of the Daresbury synchrotron. The temperature-morphology profile was then correlated with tube inversion and rheology studies of the materials to provide an understanding of the morphological development within them. The SAXS data clearly show the important transitions in the system from a stiff hexagonal gel to a mobile sol.

The sample $E_{16}B_{10}E_{16}$ 45wt.% shows a transition from a disordered sol below 20°C to a stiff hexagonal gel between 20°C and 55°C, a sol again between 55°C and 65°C and is then to a lamella form up to 90°C, after which it finally disorders in to the sol. These changes are clearly represented in the scattering patterns. Such materials have commercial interest in the manufacture of inexpensive temperature sensors and in controlled drug release.

References

[1] Brown, R.A., Masters, A.J., Price, C., Yuan, X-F., In *Comprehensive Polymer Science*; Booth, C., Price, C., Eds., Pergamon: Oxford, UK, 1989, Chapter 6.

[2] Pople, J.A., Hamley, I.W, Fairclough, J.P.A., Ryan, A.J., Komanschek, B.U., Gleeson, A.J., Yu, G-E., Booth, C., *Macromolecules*, **30**, 5721, 1997

6th Annual Workshop Abstracts

Simultaneous Medical Imaging and Diffraction Using the SRS

R.A.Lewis

CLRC Daresbury Laboratory, Daresbury, Warrington, WA4 4AD

In the field of medical X-ray imaging, a great deal of development has taken place in X-ray beam control, patient positioning, contrast agents, detectors and image processing. It is therefore perhaps surprising that there has been very little change in X-ray source technology used for medical imaging since the rotating anode X-ray generator was proposed in 1898.

It has been known for some years that using synchrotron beams to perform radiographic imaging has the potential to produce higher quality images at lower patient dose than is possible with conventional equipment. Such benefits would be of particular importance to screening programs such as the UK breast screening programme which examines more than one million women annually using standard mammography equipment. The use of the fixed wavelength produced by conventional mammography sets, coupled with a large amount of internally scattered radiation, serves to render many pathologically important features invisible. Moreover, mammography systems are optimised for the non-existent average woman, and unfortunately have very few adjustable parameters, thereby leading to a significant subset of the population for whom conventional mammography is a poor diagnostic tool. Such cases include women with particularly large or small breasts and those who have undergone previous surgery.

Results of recent tests to evaluate the imaging potential of the SRS for mammography will be presented. The use of a wavelength tunable source has allowed us to investigate the effect of X-ray wavelength on image contrast and comparisons have been performed with hospital equipment.

Finally, the results of some rather speculative but interesting experiments, in which simultaneous X-ray diffraction and imaging of breast tissue has been performed, will be presented.

Processing-Structure-Property Relations in Reaction-Induced, Phase-Separated Polymer Blends and Composites

D.Sutton[1], J.L.Stanford[1] and A.J.Ryan[1,2]

1 Polymer Science and Technology Group, Manchester Materials Science Centre, UMIST, Grosvenor Street, Manchester, M1 7HS, United Kingdom.
2 CLRC Daresbury Laboratory, Daresbury, Warrington, WA4 4AD

Solvents are used extensively in polymer processing primarily to reduce the processing temperature, thus avoiding degradation. In many cases the solvent must be removed after processing, which can be a costly and potentially hazardous procedure. An alternative method is to employ reactive solvents. Such solvents can be polymerised after shaping in the mould. Consequently, the once homogeneous, low viscosity polymer/solvent (monomer) solution is transformed to a polymer blend/composite. Polymerisation of the reactive solvent induces phase separation and phase inversion whereby the dissolved polymer becomes the continuous matrix and the reactive solvent forms a dispersed particulate phase. As the solvent ultimately becomes a structural part of the final system, by selecting the proper solvent, it may even be possible to introduce synergistic effects in the properties of the resulting blend/composite.

This poster describes the results from recent work carried out using a model system based on polyoxyethylene and styrene. Several experimental techniques have been employed so that a fundamental understanding of the phase diagram and morphology can be obtained through modelling the system's thermodynamics and kinetics. These techniques include Raman spectroscopy to monitor the extent of styrene polymerisation and simultaneous small and wide-angle X-ray scattering studies to follow the reaction-induced phase separation. Scanning electron microscopy was used to investigate blend morphologies and various optical techniques have been applied to determine the phase separation characteristics.

Crystallisation and Structure Development in Polymeric Systems

N.J.Terrill[1], J.P.A.Fairclough[1], R.J.Young[1], S-M Mai[2], C.Booth[2], I.W.Hamley[3], E.Towns-Andrews[4], B.U.Komanschek[4], R.C.Denny[4] and A.J.Ryan[1,4]

1 Manchester Materials Science Centre, UMIST, Grosvenor Street, Manchester
2 Department of Chemistry, University of Manchester, Manchester
3 Department of Chemistry and Self Organising Molecular Systems, University of Leeds, Leeds
4 CLRC, Daresbury Laboratory, Daresbury, Warrington, WA4 4AD

Semi-crystalline polymer systems are involved in all aspects of modern life from everyday uses, for example supermarket shopping bags, to more esoteric uses such as in artificial heart valves. They have recently found applications in new computer technology for data storage. The properties of these materials are usually conferred during processing where the polymer is subjected to a variety of environmental changes. One of the major structural changes that takes place is crystallisation, where the morphology of the polymer plays an integral role. During crystallisation, structure develops which controls the mechanical and aesthetic properties of the future product.

We have investigated the crystallisation process in the homopolymers, polyethylene, polypropylene, poly(ethylene oxide) and also in poly(ethylene terephthalate) by SAXS/WAXS/DSC and during the extrusion process via 2-D SAXS/WAXS. We will show how data from these experiments, analysed using CCP13 software, can lead to a better understanding of structural evolution during the manufacturing process.

The CCP13 programs FIT and LFIT have also been used to study the temperature-dependent structure within diblock copolymers in the ordered and disordered states. From the LFIT program which fits the Leibler function to the disordered fluctuation scattering, the Flory Huggins interaction parameter and the statistical segment length have been evaluated. FIT and XFIT have been used to study the change in Pearson VII peak height, position, shape, and width as a function of temperature. The results clearly show the onset of the order-disorder transition (ODT) by discontinuous changes.

How do Polymer Crystals Nucleate?

N.J.Terrill[1], J.P.A.Fairclough[1], E.Towns-Andrews[2], B.U.Komanschek[2], R.C.Denny[2], R.J.Young[1], and A.J. Ryan[1,2]

1 Manchester Materials Science Centre, UMIST, Grosvenor Street, Manchester, M1 7HS, UK.
2 CLRC Daresbury Laboratory, Daresbury, Warrington, WA4 4AD.

This study was undertaken to investigate the mechanism for nucleation in polymer crystallisation. Previous studies in this area have not been conclusive. Experiments with long induction times studied by small and wide-angle X-ray scattering (SAXS and WAXS) reveal the onset of strong long-range ordering prior to crystal growth. Rapid crystallisations studied by melt extrusion, under near industrial conditions, indicate the development of well-resolved, oriented SAXS patterns associated with long range order before the development of crystalline peaks in the WAXS region. The experimental results suggest that pre-nucleation density fluctuations play an integral role in polymer crystallisation.

Collagen Fibril Orientation in Human Cornea and Sclera

R.H.Newton, Y.Huang and K.M.Meek

Oxford Research Unit, The Open University, Foxcombe Hall, Berkeley Road, Boars Hill, Oxford. OX1 5HR

The precise orientation of the collagen fibrils in human cornea and sclera, and exactly how these two areas fuse together at the limbus, are still unknown. Quantitative information on the variation of fibril orientation with depth in these tissues is entirely lacking, but is of clinical relevance.

Corneal transplants usually use donor corneas with no regard to their orientation with respect to the remaining host material. It is not known why some of these transplants are not successful, but it may in some cases be due to the collagen orientation being wrong. A preliminary clinical trial in America suggests that donor to host alignment may play a role in the magnitude of post-surgical astigmatism [1]. A major clinical trial is now underway based in Manchester. Weakening and elongation of the sclera is implicated in the formation of myopia [2] and the

mechanical properties of the sclera in different directions will depend greatly on the fibril orientation in the tissue. Changes in the collagen orientation in different parts of the sclera during the development of myopia have not been studied in detail.

Using synchrotron X-ray diffraction, Meek *et al.* [3] found two preferred directions in human corneal stroma, inferior-superior and medial-lateral, and found that the preferred directions were more pronounced in the posterior stroma than the anterior stroma. We are currently extending this work to give quantitative orientation distributions with greater depth resolution across the cornea and sclera.

Normal human cornea and sclera were supplied by UKCTS Eye Bank in Bristol and X-ray diffraction patterns collected at station 7.2. A pattern was collected from the centre of an intact full thickness cornea. A thin layer was then dissected from the anterior surface and patterns collected both from the resulting lenticule and from the remaining tissue. A further layer was then removed and further patterns collected. In total, the cornea was dissected into 4 approximately equal thickness layers.

The sequence of patterns shows the change from an approximately isotropic distribution in the anterior cornea to a biaxial distribution in the posterior cornea.

Preliminary work on full-thickness sclera was also carried out. A globe was opened out into four segments and patterns collected at points spaced by 2mm along a transect from the limbus to the optic nerve.

The preliminary work has shown that it is possible to obtain orientational information from diffraction patterns taken from corneal lenticules of around 100μm thickness and that X-ray diffraction can also demonstrate changes in scleral collagen orientation around the ocular globe. We are in the process of carrying out further work to map in detail the fibril orientation with depth around the entire ocular globe.

References

[1] Rapuano, C.J., Dana, M.R. Gomes, J.A.P. and Laibson, P.R. (1995) *Inv. Ophthal. Vis. Sci.* **36**(4), S653

[2] Curtin, B.J., Iwamoto, T. and Renaldo, D.P. (1979) *Arch. Ophthalmol.* **97**, 912-915

[3] Meek, K.M., Blamires, T. Elliott, G.F. Gyi, T.J. & Nave, C. (1987) *Current Eye Research* **6**(7), 841-846

Background Correction of Fibre Diffraction Patterns

M.Ivanova and L.Makowski

Florida State University Tallahassee, FL 32306-3027

Background correction of fibre diffraction patterns is problematic due to the intrinsic nature of the diffracting specimen: the axes along which diffracting particles exhibit order are not strictly parallel to each other. This effect causes arcing of the reflections and overlapping of layer-lines at high radii. Because of this, the estimate of background at high resolution can be ambiguous.

We have designed and tested a procedure which allows estimation of the background from the diffraction pattern, based on the assumption that the spatial frequencies of the background and the layer line intensities are well separated. Background correction and data extraction are made by application of a low pass filtering followed by angular deconvolution of layer-line intensities. This process is iterative and starts with overestimated background and underestimated intensities, which are improved at each cycle until a best fit between calculated and observed data is obtained. This method was applied to X-ray fibre diffraction patterns from filamentous bacteriophages to correct for the background and to calculate the intensities along the layer-lines.

Optimising Synchrotron Facilities for Diffraction and Scattering

C.Nave

CLRC Daresbury Laboratory, Daresbury, Warrington WA4 4AD, UK

A method is presented for specifying the optimum X-ray source, optics and detectors for diffraction and scattering. Simply asking for the highest flux or highest brightness is misleading. A better definition of the requirements would be to have the maximum flux into the phase space volume required by the

specimen. A proper evaluation of the requirements should therefore start from the characteristics of the range of specimens which are to be studied. A graphical phase space diagram is derived to illustrate how various sources, optics and detectors are matched to parameters such as specimen size and periodicity. The perfection of the sample should also be considered as this can affect the spread of diffracted beams from the sample. In the case of crystals, a simple 3 parameter model can be used to describe sample perfection. For fibres, the coherent length of the particles within the fibre is relevant.

These considerations have consequences for the choice of source (X-ray generator, bending magnet, undulator or multipole wiggler), optics and detectors. Typical issues are whether there is a limit to the source emittance required or the size of an area detector system. The various considerations will be illustrated by describing possible facilities on DIAMOND, the proposed new UK synchrotron source.

Chain Mobility in Polymers; a Novel Route for Welding and Processing

S.Rastogi, L.Kurelec and P.J.Lemstra

Eindhoven Polymer Laboratories, Eindhoven University of Technology, The Netherlands

The motion of chains in quiescent polymer melts is confined to a reptative diffusion along the contour length as proposed by De Gennes. In the constitutive equations based on the concept of chain reptation, it is assumed that the longest relaxation times in polymer melts correspond to the reptative motion of complete chains. In the case of Ultra High Molecular Weight Polyethylene, UHMW-PE, possessing a weight average molar mass over 103kg/mol, the experimentally determined relaxation time exceeds more than 104 seconds. Processing of UHMW-PE via conventional routes is virtually impossible due to the high molar mass and high melt viscosity. Since the mechanical and physical properties like toughness and abrasion resistance also increases with the molar mass, UHMW-PE is used in high performance products such as hip-joint prostheses where it constitutes the interface between the implanted metal bar and the bone. But high melt viscosity of the UHMW-PE imposes problems in welding (*i.e.* fusion of the particles) and processability of the material, thus limiting the lifetime of the product.

In this colloquium, a detailed study concerning the chain mobility in the gel crystallised films, nascent materials of UHMW-PE at the atmospheric and the elevated processable pressures will be highlighted. It will be demonstrated that the enhanced chain mobility below the melting temperature can be used as a route to circumvent the problems stated above.

The Variation in Cell Parameters of Unoriented and Drawn Branched Polyethylenes According to Branch Type, Content and Distribution

A.M.E.Baker and A.H.Windle

Department of Materials Science and Metallurgy, Pembroke Street, Cambridge, CB2 3QZ

Experimental data from branched polyethylenes are usually analysed with respect to branch type and content. Differences in the distribution of branches between samples are not generally considered in such analyses, principally because until recently a means of determining the branch distribution has not been possible. A parameter describing the extent of heterogeneity in branch distribution of polyethylenes [1] is now possible using TREF (temperature rising elution fractionation).

We have used X-ray diffraction to investigate the variation in cell parameters of branched polyethylenes according to branch type and content (from ^{13}C NMR studies) and, for the first time, branch distribution (from TREF work). Fifteen commercial grades were investigated, in both powder and fibre form. We were therefore able to examine possible differences caused by sample orientation.

All samples showed an increase in a and b cell parameters with increasing branch content; this effect is well known [2]. The fibre samples showed a broader range of lattice parameters and a small decrease in the c parameter with branch content was also detected, as has been reported previously [3]. The a parameter of the fibre samples indicated a dependence on branch type; which has not been noted before. Generally, however, there appeared little or no effect of branch type for ethyl and longer branches. Of greatest interest was the slight but significant dependence of lattice parameters on branch distribution seen across all samples: the more

random the distribution for similar branch contents, the greater the expansion seen in *a* and *b* lattice parameters and the contraction seen in *c* (fibre samples only). The unit cell expansion with increasing levels of branching was attributed partly to a reduction in crystallite size (surface stress on thinner lamellae [3]) and partly to a limited incorporation of branches into the crystallites leading to structural strains and distortions. Such branch incorporation was also indicated by changes seen in some diffracted intensity ratios, and reinforced by molecular modelling reported elsewhere [4].

References

[1] Bonner, J. G., Frye, C. J. & Capaccio, G. (1993). *Polymer*, **34**, 3532.
[2] Swan, P. R. (1962). *J. Polym. Sci.* **56**, 403.
[3] Howard, P. R. & Crist, B. (1989). *J. Polym. Sci. (Phys.)* **27**, 2269.
[4] Baker, A. M. E. (1996). Ph.D. Thesis, University of Cambridge.

Morphological Aspects of the Biodegradation of Poly(glycolic acid)

E.Norton and R.E.Cameron

University of Cambridge, Department of Materials Science and Metallurgy, New Museums Site, Pembroke Street, Cambridge, CB2 3QZ, UK

Poly(glycolic acid) is a semi-crystalline polymer which degrades in water via a bulk hydrolytic mechanism. It is totally biodegradable and produces no harmful degradation products, hence it has found use in biomedical applications such as resorbable sutures, bone fixation devices and is being investigated as a potential material for controlled drug delivery devices.

The inter-relationships between morphology and degradation are currently ambiguous, yet of critical importance in the design of biomedical devices where prediction and control of degradation are essential. We present a study of the biodegradation of poly(glycolic acid) at a morphological level, relating microstructural features to changing physical and mechanical properties. We have monitored the changing morphology and properties of samples after in vitro degradation, using simultaneous small and wide angle X-ray scattering experiments, scanning electron microscopy, thermal analysis and spectroscopy.

Oriented Diblock Copolymer Solutions.

J.P.A.Fairclough[1], A.J.Ryan[1,4], H.Li[2], S-M.Mai[2], C.Booth[2], I.W.Hamley[3], J.Pople[3]

1 Manchester Materials Science Centre, UMIST, Grosvenor Street, Manchester, M1 7HS
2 Department of Chemistry, University of Manchester, Manchester
3 Department of Chemistry and Self Organising Molecular Systems, University of Leeds,
4 CLRC, Daresbury Laboratory, Daresbury, Warrington, Cheshire.

Solutions of poly(oxyethylene)-poly(oxybutylene) di- and triblock copolymers in water have been studied by small angle X-ray scattering (SAXS), small angle neutron scattering (SANS) and rheology. As the concentration of block copolymer in solution is increased the micelles transform into soft gel structures of interpenetrating micelles. As the concentration of polymer is increased further, these change to a hexagonally packed cylindrical morphology, then to lamellar morphology. The poly(oxyethylene) block is known to be hydrophilic, whereas the poly(oxybutylene) is hydrophobic. As a result, the poly(oxyethylene) block is solvated by the water with the poly(oxybutylene) becoming the core of the micelle. We have mapped extensive areas of the polymer/water phase diagram as a function of concentration and temperature. The phase diagram of the triblock copolymers by rheology exhibit complex phase diagrams as opposed to the diblock copolymer due to the formation of bridges in the triblock copolymers at low concentrations. Results of SAXS and SANS of oriented samples will be presented together with rheometric results.

Rejection and Co-crystallization in PET/PEN Random Copolymers

G.E.Welsh and A.H.Windle

Department of Materials Science and Metallurgy, University of Cambridge, Pembroke Street, Cambridge, CB2 3QZ

Poly(ethyleneterephthalate)/Poly(ethylenenaphthalene-2,6-dicarboxylate) (PET/PEN) random copolymers can be crystallized at all compositions by drawing above the glass transition temperature. X-ray fibre diffraction shows that the crystalline structures of the resulting fibres may be divided into three categories: a PEN structure in the range 0-20% PET, a structure in

which the lateral packing of chains is similar to that of PEN, in the range 20-70% PET, and a PET structure in the range 70-100% PET. The crystal melting point of the fibres decreases with composition as 50% PET is approached from either side. This could be the result of either rejection or co-crystallization, so X-ray fibre diffraction and computer modelling have been used to investigate which of these is taking place at a number of different compositions.

Diffraction patterns calculated from model random copolymer crystallites show that if random sequences are included at all compositions then layer line positions and intensities should vary with composition. Also, as the composition approaches 50% PET, the layer-lines should become more diffuse and less sampled.

In this work the layer-line positions and intensities from diffraction patterns of samples of different compositions have been measured and compared with those obtained from models in which it is assumed that there is co-crystallization at all compositions. This has confirmed that co-crystallization occurs in the range 20-70% PET but seems to indicate that rejection is taking place outside this range.

Structural Organisation of Flower Bulb Lectins: How Important is the Tetramer?

P.J.Rizkallah[1], M.K.Sauerborn[1], J.G.Grossmann[1], L.M.Wright[1], C.D.Reynolds[2]

1 CLRC Daresbury Laboratory, Warrington, Cheshire, WA4 4AD
2 Biophysics Dept, Liverpool John Moores University, Byrom Street, Liverpool, L3 3AF

Occurrence: Lectins are common in nature and used by all phyla for many purposes. They recognise sugars, and are therefore involved in sequestering these metabolites for the normal functioning of the organism.

Properties: The affinity for sugars allows lectins to bind to cells by attaching themselves the glycosylated (sugared) proteins on cell surfaces. They bridge between cells if they are multimeric, with each binding site attached to one cell. This is called agglutination, and is widely used in medicine for blood typing: Lectins from different plants bind specifically to only one type of blood cell, causing agglutination.

Binding to the sugars on the surface of human T-cells triggers an immune reaction similar to the reaction to any ordinary disease. The difference is that pathogens activate 0.1% of the T-cells, while lectins activate 70 to 80%. This has been used as a diagnostic tool for assessing the immune response of patients with undermined immunity. The test can only be done in vitro, because debris of killed cells would otherwise cause severe, potentially fatal, allergy.

Flower bulb lectins have the specificity to mannose, a sugar abundant on the surface of HIV, localised at GlycoProtein 120, GP120. The virus uses the sugar coat to escape the immune system, while hiding a patch that forms the site of recognition for CD4, a protein on the surface of T-cells. Once recognised, T-cells are infected by the virus. But lectins stick to GP120 mannose, and block binding of CD4 by steric hindrance. This makes them anti-viral, at least in vitro.

Structure: Lectins from the bulbs of amaryllis, bluebells and daffodils were crystallised and their structure solved with X-ray crystallography. They are highly homologous, and show a unique fold, recently identified in snowdrop lectin. The monomer is made up of three beta sheets, 4 strands each, wrapped around an internal 3-fold axis of pseudo-symmetry: Beta-prism, Type II. The last strand of this motif peels off, and is exchanged with the equivalent strand from a neighbouring molecule, restoring the beta-sheet there. The dimer that is thus formed is very tight, with a special lock-and-key mechanism. Two dimers coalesce, in the crystals, to make a tetramer. Tetramers are then involved in a number of interactions that build up a lattice. The tetrameric interface shows a hydrophobic patch, which is hidden away from the solvent by tetramer formation. There are mutations, at that point, in the bluebell sequence, to make this interface less hydrophobic. The integrity of the cluster in solution was then tested with solution scattering. Theoretical curves for dimers and tetramers were calculated, and compared with the experimental curves, showing that daffodil lectin is tetrameric, while bluebell lectin is dimeric. Calculations of the radius of gyration also support that. The cluster forming ability may have some importance in determining the strength of anti-HIV activity in this class of protein.

Tobacco Mosaic Virus Assembly Revisited

B.Bhyravbhatla, R.Diaz-Avalos and D.L.D.Caspar

Institute of Molecular Biophysics Florida State University Tallahassee FL 32306-3015

Tobacco mosaic virus (TMV) is the paradigm of a self-assembly structure. Its dissociated coat protein can be reassembled in variant disk aggregates as well as in the native helical structure with or without the viral RNA. The intact TMV particle is the only helical macromolecular assembly yet solved to atomic resolution by X-ray fibre diffraction. The coat protein structure and its side-to-side packing in the virus helix, as determined by Namba and Stubbs in 1986-89, is similar to that in the crystalline four-layer disk, first modelled by Bloomer *et al* in 1978 from the pioneering X-ray crystallographic analysis in Klug's laboratory. However, the packing between the disk layers is quite different from that between the turns of the 23Å pitch virus helix. The nucleating aggregate that initiates the helical virus assembly, which had been presumed to be a two-layer disk, now appears to be a short helix segment whose axial growth is limited in the absence of the stabilizing RNA. To investigate the switching mechanisms involved in the polymorphic protein interactions, we have re-refined the atomic structure of the four-layer disk aggregate against 2.4Å resolution cryocrystallographic data, and we have reconstructed a three-dimensional image of the stacked-disk aggregate at 10-15Å resolution from electron cryomicrographs. Furthermore, we have collected fibre diffraction data with synchrotron radiation from tilted nematic liquid-crystalline specimens of intact TMV particles that extend to 1.2Å resolution near the meridian from the best oriented aged specimens; analysis of the high resolution fibre diffraction will require improvements in our methods of data processing. From the refined crystal structure of the four-layer disk, it has been possible to trace the previously invisible disordered near-axial loops of the polypeptide chain, which appear significantly different in the two rings of the asymmetric unit. The conformation of the well-ordered portions of the protein are similar in the two layers, although the connections between the dihedrally related A-ring pair are entirely different from those between an outer B-ring with a central A-ring. Water-mediated interactions predominate between the layers, most notably between the large overlapping area of the central A-ring pair which involve linkages only through one or more ordered water molecules. Our comparison of the three-dimensional image reconstruction of the stacked-disk aggregate with models based on the crystalline disk structure has established that the two-layer unit which builds the stacked disk has a structure very close to that of the dihedrally-related A-ring pair. This result conclusively demonstrates that the symmetry of the stacked disk aggregate is bipolar rather than polar, as previously inferred. Once this aggregate has formed, it will not come apart under conditions that lead to dissociation of other TMV protein assemblies. The differences in stability and packing arrangement of different TMV protein aggregates does not appear to involve significant alteration in the subunit conformation, but does display the adaptability in the protein interactions.

X-ray Diffraction/Scattering Studies on Plant Pro-lamellar Bodies (PLB)

W.P.Williams[1], T.Brain[1], E.Selstam[2], J.G.Grossmann[3]

1 King's College, London
2 University of Umea, Sweden
3 CLRC Daresbury Laboaratory

PLB are highly organised membrane systems found in sub-cellular organelles (etioplasts) formed in the leaves of plant seedlings germinated in the dark. On exposure to light, etioplasts convert into the chloroplasts found in normal leaves. As part of this process, the PLB are converted into the internal thylakoid membrane system that contains the photosynthetic light-harvesting and energy transducing systems of the chloroplast. The PLB is in effect a storage body that contains the membrane lipids and precursors of the main photosynthetic pigments. Its biological importance lies in its role as a model system used in the study of the developmental biology of chloroplasts. The PLB are made up of the four chloroplast thylakoid membrane lipids (MGDG - monogalactosyl diacylglycerol, DGDG - digalactosyl diacylglycerol, SQDG-sulphoquinovosyl diacylglycerol, PG - phosphatidyl diacylglycerol), proto-chlorophyllide (a precursor of chlorophyll) and the protein protochlorophyllide oxidoreductase. In terms of structure, it is one of the very few known examples of a natural cubic membrane system. Our studies, which have been carried out on PLB isolated from maize, have been aimed at characterising the PLB structure using a

combination of electron microscopy and SAXS measurements. The electron microscopy data suggests that the PLB are made up from a highly convoluted lipid bilayer, in the form of tetrapodal units, which are joined together to form a diamond cubic lattice with a unit cell of about 70nm. The X-ray diffraction/scattering patterns are consistent with this view. We are able to identify a set of low-angle diffraction maxima indexing to a diamond cubic lattice of similar unit cell size and a set of wider angle scattering peaks that appear to arise from the individual tetrapodal units.

Circular Dichroism Studies of DNA in Fibres and Solutions

C.Boote[1], Y.Hong[1], R.C.Denny[2,3], T.Forsyth[1], D.T.Clarke[3], G.Jones[3]

1 Physics Department, Keele University, Staffordshire, ST5 5BG, UK
2 Blackett Laboratory, Imperial College, London
3 CLRC Daresbury Laboratory, Warrington WA4 4AD

A preliminary circular dichroism study of DNA in fibres and solutions has been carried out on beamline 3.1 at the Daresbury SRS. The aim of the these experiments is to relate DNA conformations as identified by fibre diffraction to corresponding CD spectra so that a set of CD "fingerprints" can be used to identify different DNA conformations in more complex systems such as DNA protein complexes. In the experiments that have been undertaken so far, work has focused on the relationship between CD spectra recorded from fibres and those recorded in solution.

Making Hairpins from Rings and Chains

A.J.Ryan, J.Cooke, J.P.A.Fairclough

Manchester Materials Science Centre, UMIST, Grosvenor Street, Manchester, M1 7HS

The crystallisation of cyclic polyethylene oxides is compared to their linear precursors and the enthalpy and entropy of chain folding is estimated from the SAXS/WAXS/DSC. The crystallisation of a series of diblock poly(oxyethylene-oxybutylene) copolymers has been studied by combined SAXS/WAXS/DSC. Polymers were crystallised from either the disordered (fluctuating) melt or the ordered melt depending on the molar mass. There was an increase in the characteristic length scale on crystallisation of the polyoxyethylene block which implies stretching of the amorphous polyoxybutylene block. Low molar mass copolymers crystallised with extended stems. Higher molar mass copolymers had folded stems whose equilibrium length was determined by the balance between the enthalpy of polyoxyethylene chain folding and the entropy of polyoxybutylene stretching. The crystallisation process gave crystals with integral folds which showed a quantisation in the dependence on the characteristic length with crystallisation temperature. The stem lengths observed in homo-polyoxyethylene are three times larger than in the copolymers due to the polyoxybutylene acting as an entropic piston.

High-Angle Neutron Fibre Diffraction Studies of A-DNA

M.W.Shotton[1], L.H.Pope[1], V.T.Forsyth[1], P.Langan[2], R.C.Denny[3], M.Dauvergne[4], U.Giesen[4], W.Fuller[1]

1 Keele University, Staffordshire, UK. ST5 5BG.
2 Institut Laue Langevin, Grenoble, France.
3 Daresbury Laboratory, Warrington, UK.
4 E.M.B.L., Grenoble, France.

A high-angle neutron fibre diffraction study of the hydration of A-DNA has been performed using the single crystal diffractometer D19 at the Institut Laue-Langevin, Grenoble. The sample was prepared using deuterated DNA extracted from E. Coli cells cultured on deuterated nutrients. In common with our previous neutron fibre diffraction studies of DNA, this work exploits the ability to isotopically replace H_2O around the DNA by D_2O. However, this study benefited additionally from the fact that the hydrogen atoms which are covalently bonded to carbon atoms in the DNA sugars and bases were replaced by deuterium, so that incoherent scattering and absorption effects were minimised. Successive cycles of Fourier synthesis and Fourier difference synthesis allowed water peaks to be identified and their positional and occupancy parameters to be refined against the observed diffraction data. The results confirm the main hydration features noted in our earlier studies [1] with a clear network of water running along the inside edge of the major groove linking successive O1 phosphate oxygen atoms. The central core of water running along the axis of the double helix is very much clearer in this work. Additionally, this study shows chains of ordered water lying in the centre of the major groove.

Simultaneous SAXS and Rheological Characterization of Polymer Systems in Shear Flow

J.A.Pople[1], I.W.Hamley[1], J.P.A.Fairclough[2], A.J.Ryan[2]

1 School of Chemistry, University of Leeds, Leeds LS2 9JT, UK
2 Manchester Materials Science Centre, Grosvenor St., Manchester M1 7HS, UK

The development of a rheometric system suitable for the characterization of polymeric systems in situ by small angle X-ray scattering (SAXS) and rheology is presented. The rheometer comprises a shear sandwich arrangement in which a central insert oscillates between two fixed outer plates to generate a simple shearing field, in which the dynamic moduli are measured as a function of the deformation conditions. Apertures machined in the plates permit transmission of the X-ray beam, and therefore simultaneous determination of the structural characteristics of the polymer system.

The phase behaviour of micellar copolymer gels of polyoxyethylene and polyoxybutylene has been studied as a function of temperature and copolymer concentration. A rich variety of phases is observed: a body centred cubic (bcc) phase, a face centred cubic (fcc) phase and a hexagonally packed rod (hex) phase are observed in all concentrations studied, as the temperature is increased. The transition from the bcc to fcc phase arises from the temperature-induced thinning of the coronal layer of the micelle leading to shorter range intermicellar interactions, and thus favouring the fcc structure.

The application of large amplitude reciprocating shear results in a reduction of the dynamic moduli, typically by two orders of magnitude, and a sharpening of the diffraction rings in the SAXS patterns, indicating an increase in the degree of order. Modest levels of orientation (order parameters $\langle P_2 \rangle$ ~0.25) are realized when a 38% copolymer gel is sheared in the hex phase at 10/s. Upon cessation of the shear field the dynamic moduli recover rapidly as the defects are annihilated, whilst the induced orientation decays very slowly.

Determination of the Optimum X-ray Energy for Mammography using Synchrotron Radiation

S.M.Slawson, G.R.Mant, E.Towns-Andrews, C.J.Hall, R.A.Lewis, A.Hufton and G.Diakun

CLRC Daresbury Laboratory, Daresbury, Warrington, WA4 4AD

X-ray mammography is one of the most widely used diagnostic techniques in medicine, yet despite the wide use of the technique, very little work has been performed on the X-ray attenuation of the various normal and diseased breast tissues. It is these X-ray attenuation coefficients which determine image contrast in mammograms and accurate knowledge of them is necessary in order to optimise any mammography system and to calculate the dose required by each patient. To date, the most accurate work on these studies has been published by Johns and Yaffe, (1987). The accuracy of this work was limited by the use of a non-tuneable source of X-rays and the small number of samples studied. The results indicated that optimum contrast between diseased and normal tissue is obtained using energies below 25keV. However, their data did not extend below an energy of 18keV. The data presented here, used an energy tuneable source, *i.e.* a synchrotron, to determine linear X-ray attenuation coefficients, by normal breast tissue, obtained from breast reduction mammoplasty, over the range of energies 15 to 25keV. The results obtained clearly demonstrated that differences in the attenuation coefficients increased with decreasing energy.

Unravelling the Protein Folding Problem Using Stopped-flow Techniques

G.R.Jones

CLRC Daresbury Laboratory, Daresbury, Warrington, WA4 4AD

The progress in studying early events in protein folding using non-crystalline diffraction and other synchrotron techniques is reviewed. The general goal of the work is to relate the overall collapse of the structure to form a globular unit, as studied by X-ray solution scattering, to the formation of secondary structure as determined by SR VUV circular dichroism techniques. The scattering technique pushes the limits of what is currently possible in that

protein concentrations by necessity have to be less than 1mg/ml and time resolutions of a millisecond are required.

The Molecular Fine Movement of Muscle Contraction

M.A.Ferenczi[1], P.Brown[1], R.Burns[1], O.N.Bershitskaya[2], G.I.Mashanov[2], A.K.Tsaturyan[3], S.Y.Bershitsky[2]

1 National Institute for Medical Research, Mill Hill, London NW7 1AA
2 Urals Branch of the Russian Academy of Sciences, Ekaterinburg
3 Institute of Mechanics, Moscow State University.

Single cells isolated from vertebrate skeletal muscle can be made permeable by removing or puncturing the cell membrane. These muscle fibres contain the contractile machinery only: sets of repeating units of interdigitating protein filaments made of myosin and actin. The myosin filaments consist of elongated myosin molecules which, at one end, have a globular region which binds to, and detaches from, the actin filaments. These globular regions are called cross-bridges. The regular packing of the filaments means that low-angle X-ray diffraction reveals the details of the filaments' packing, and during contraction, changes in the diffraction pattern are seen which provide information about movement of the proteins responsible for contraction. Using permeabilized muscle cells, the contractile state of the muscle can be changed rapidly, allowing the observation, often with a high time resolution, of the corresponding structural changes. Two techniques will be described, which have been used to rapidly change the state of muscle fibres, and hence to observe the molecular movements underlying force generation.

Using caged-ATP, a muscle fibre in rigor can be activated using the sub-millisecond photolytic generation of ATP, the cell's molecular fuel. Changes in the diffraction patterns occur over a range of time-courses. Most of the larger changes in the patterns are faster than force generation, indicating that one is observing molecular rearrangements resulting from ATP binding to the cross-bridges.

The second method is perturbation of the muscle state by rapidly increasing the temperature. This temperature jump technique (T-jump) is achieved by passing an electric current through the muscle fibre. A change in temperature from 6 to 18°C causes tension to increase by a factor of 1.7 without causing any other change to the chemical environment of the muscle proteins, or any change to the physiological state of the muscle cell. Thus the changes in the diffraction pattern resulting from the temperature jump result from the structural changes responsible for the tension increase, without perturbation from other processes in the cell. The main observed feature is an increase in the intensity of the first actin layer-line, indicating that the increase in force is accompanied, and by inference - probably caused, by an increase in the fraction of cross-bridges rigidly attached to the actin filaments. As the total number of attached cross-bridges does not change, it appears that force generation is brought about by cross-bridges weakly attached to actin becoming attached in a stereospecific manner.

Structure of the Capsid of Pf3 Inovirus Determined From 3.1Å Fibre Diffraction Data.

L.C.Welsh, M.F.Symmons, D.A.Marvin and R.N.Perham

Department of Biochemistry, University of Cambridge, Tennis Court Road,Cambridge, CB2 1QW, U.K.

X-ray diffraction data recorded from magnetically aligned fibres of Pf3 virions have been used to determine the structure of the major coat protein within the capsid by molecular replacement from a model of the major coat protein of the structurally well defined low temperature symmetry form of the Pf1 strain of Inovirus [1]. The Pf3 capsid has the same helical symmetry as that of the higher temperature form of the Pf1 virion but Pf3 virions do not undergo a temperature induced helical symmetry transition of the kind observed for Pf1 virions.

An initial 5Fo-4Fc Fourier synthesis electron density map of the Pf3 major coat protein was calculated from the Pf3 fibre diffraction data using phases from an all alpha helix model of the Pf1 major coat protein stripped of side-chain atoms. A number of initial atomic models of the Pf3 major coat protein consistent with both the observed fibre diffraction amplitude data and the initial Pf3 major coat protein electron density map could be built.

It was possible to discriminate between these models on the basis of the level of sequence homology resulting from their structural alignment with the Pf1 major coat protein sequence. The existence of a large

number of well determined globular protein structures has led to the derivation of a number of empirical rules for validating models of protein structures and two such methods were used to discriminate between the remaining Pf3 models [2,3].

Three of the initial Pf3 models emerged as viable candidates for the structure of the Pf3 capsid, and each was refined against the observed fibre diffraction data using both Cartesian coordinate and torsion angle coordinate simulated annealing refinement protocols. Refinement using torsion angle dynamics results in a large reduction in the number of degrees of freedom of the models [4]. One of the refined models was consistently favoured by all the criteria by which the models were judged and this was taken as the best model of the structure of the Pf3 capsid. This model is also the model closest to the Pf1 backbone coordinates.

The structure of the Pf3 capsid is very similar to that of Pf1 and possesses a similar network of non-polar inter-subunit van der Waals contacts between residues in the central regions of the major coat proteins. However, there are significant differences in the structures of the N and C-termini of the proteins. In particular the N-terminus of the Pf3 major coat protein is in an alpha-helical conformation whereas that of Pf1 is not [1].

The structure of the C-terminal region of the Pf3 capsid shows that there must be significant DNA/protein interactions in the virion involving both charged side-chains and aromatic side-chains, whereas the DNA/protein interactions in the model of the Pf1 virion predominantly involve charged side-chains. This difference in DNA/protein interactions may result in differences in the low-frequency dynamics of the virions and thereby be responsible for the absence of a temperature transition in the Pf3 virion.

References

[1] Gonzalez, A., Nave, C., & Marvin D.A. (1995). *Acta Cryst.* **D51**, 792-804.

[2] Eisenberg, D. & McLachlan, A.D. (1986). *Nature* **319**, 199-203.

[3] Lüthy, R., Bowie, J.U. & Eisenberg, D. (1992). *Nature* **356**, 83-85.

[4] Rice, L.M. & Brünger, A.T. (1994). *Proteins* **19**, 277-290.

Data Analysis of 2D-SAXS Patterns with Fibre Symmetry from some Thermoplastic Elastomers

N.Stribeck

Institut für Technische und Makromolekulare Chemie,University of Hamburg, Bundesstr.45, D-20146 Hamburg

2D-SAXS patterns of samples with fibre symmetry contain the complete information on the microstructure, which can be obtained utilizing the scattering method. In the case of thermoplastic elastomers this microstructure is built from hard domains dispersed in a soft matrix. Straining such elastomers, one observes scattering patterns with fibre symmetry. Since synchrotron radiation sources and advanced detectors are available, one is able to resolve the details of these patterns with high accuracy. Changes of reflection positions and shapes can be studied easily. A quantitative analysis of the complete structure information, on the other hand, requires sophisticated image pre-processing. Based on modern tools for scientific data analysis (PV-WAVE, IDL), the effort is tolerable. Direct fitting of the two-dimensional image information with a structural model appears to be expensive, but is not necessary in every case. According to Bonart's notion of dividing the fibre diagram in a "longitudinal structure" and a "transversal structure" component [1], it is possible to extract two curves from the image by appropriate projections. These curves must conform to a one-dimensional structural model. Curve fitting, on the other hand, is a well-established technique. Scattering images, which have been recorded during the straining of thermoplastic elastomers, serve for demonstration purpose [2]. SBS block copolymers and polyether esters (*e.g.* Arnitel™) have been studied. In the proposed concept for data analysis I try to realise OOP-methods within PV-WAVE: Images are stored in a complex structure. Methods, written in the programming language of IDL, act on such an image structure. To some extent the state of the image structure reflects the state of analysis of the picture. So it is possible to place a deliberate number of images in different states of analysis "on the desktop", and for the analysis it is possible to choose the order of objects and transformation steps freely. Modification of the steps (procedure code) can be done "on the fly", since the code is interpreted. Masks (*i.e.* images containing only values of either

"0" or "1") have turned out to be a useful concept for the primary image processing. Using this concept methods for image alignment and image improvement can easily be implemented. Powerful 2D-extrapolation routines implemented in PV-WAVE (not in IDL) serve for the purpose of covering the central blind spot and for the purpose of outward extrapolation.

References

[1] Bonart R. (1966) *Kolloid Z u Z Polymere* **211** 14-33

[2] Stribeck N., Sapoundjieva D., Denchev Z., Apostolov A.A., Zachmann H.G., Stamm M., Fakirov S. (1997) *Macromolecules* **30** 1329-1339

CCP13 Program Updates

R.C.Denny

Imperial College & CLRC Daresbury Laboratory

Two CCP13 programs, XFIT and XFIX, have been made more user-friendly by the addition of OSF/Motif-based graphical user interfaces (GUIs). Improvements to XFIT will be discussed with a demonstration of the "Auto" option for fitting sequences of frames of data. The new XFIX interface will be introduced and a demonstration of some preliminary processing of a fibre diffraction pattern will be given. Some improvements to FTOREC and LSQINT and the potential uses of Java for CCP13 will also be discussed.

Software Development via Interactive Graphics

R.M.Hilmer

dCode Software Tools, Inc.

A description will be presented of the dCode(TM) package, which allows a programmer to develop software using interactive graphics. The user draws structured flowcharts and defines a database, and dCode(TM) produces compileable code automatically. Some discussion will also be given concerning present and future development plans for dCode.

Instrumentation for X-ray Fibre Diffraction Under Industrial Processing Conditions

A.Mahendrasingam[1], C.Martin[1], S.Bingham[1], D.Hughes[1], W.Oatway[1], E.Healey[1], W.Fuller[1], D.J.Blundell[2], D.H.MacKerron[2], R.J.Oldman[3], R.J.Rule[2], P.Engstrom[4], C.Riekel[4]

1 Department of Physics, Keele University, Staffs. ST5 5BG,UK

2 ICI Films,PO Box No.90, Wilton Research Centre, Middlesbrough, Cleveland, TS90 8JE, UK

3 ICI Chemicals and Polymers Ltd, Runcorn Technical Centre, Runcorn, Cheshire WA7 4QD, UK

Recent developments at the Synchrotron Radiation Source (SRS) Daresbury and the European Synchrotron Radiation Facility (ESRF) Grenoble have allowed major advances in the structural information which can be obtained in fibre diffraction studies of polymer materials. These advances are illustrated in this report by recent work of the Keele Fibre Diffraction Group. Much of this work has been done in collaboration with ICI plc. The exploitation of the high brilliance of the synchrotron sources to record and display in real-time the variation in diffraction during drawing and annealing of polymer materials with exposure times as short as 40 milliseconds synchronised with a continuous video record of changes in the gross appearance of the specimen.

A Simultaneous SAXS/WAXS and Stress/Strain Study of Polyethylene Deformation at High Strain Rates.

D.J.Hughes, A.Mahendrasingam, W.B.Oatway, E.L.Heeley, C.Martin and W.Fuller

Department of Physics, Keele University, Staffordshire, ST5 5BG, UK

An experimental system has been commissioned which allows the collection of time-resolved simultaneous two-dimensional SAXS/WAXS and stress/strain data with a temporal resolution of 40ms during the drawing of synthetic polymers. X-ray data collection is achieved via two CCD-based area detectors which are positioned in order to maximize the amount of scattering that can be observed from a particular sample. True stress/strain measurements are obtained from video extensometer and load cell

measurements. The system was used at the Daresbury SRS to study the structural changes which occur in a sample of isotropic high-density polyethylene when subjected to an overall strain rate of about $3s^{-1}$. It is shown that the onset of both a partial stress-induced crystal phase change and micro-voiding in the sample can be directly correlated to the point of yield in the true stress/strain curve.

New Insight into The Crystallization Behavior of Polymers and Fibres via Time-Resolved Synchrotron X-ray Measurements and Novel Data Analysis Techniques

B.S.Hsiao

DuPont CR&D

Several new insights into the structural and morphological behavior of crystalline polymers and fibres during phase transition and deformation have been obtained via simultaneous small and wide-angle X-ray scattering (SWAXS) methods using synchrotron radiation in conjunction with novel data analysis techniques (1D and 2D). These findings are summarized as follows: (1) Under isothermal crystallization conditions and in the quiescent state, the lamellar long period (from SAXS) was found to decrease with time for most polymers. Further analysis using the correlation function revealed that the average crystal lamellar thickness decreases in semi-stiff polymers but can increase slightly in some flexible polymers (lamellar thickening). We ascribe the decrease in long period and lamellar thickness as due to secondary crystallization in the strained melt which produces thinner lamellae. The WAXS results also indicated that the crystal density increases with time. (2) During fibre spinning and deformation, three phases (amorphous, slush, and crystalline) are evident in the chosen polymer systems (nylon66, PET, PE and PVDF). We found that during spinning at higher speeds (500-1000mpm), the crystalline phase in nylon66 fibres is absent, which only develops after the wind-up and post-treatments. Heat-drawing of a fully crystallized nylon66 fibre often leads to a premelting process proceeding to the Brill transition. During spinning at low speeds (10 to 60mpm), we confirmed the occurrence of SAXS signals prior to WAXS in PE and PVDF. This finding suggests that the formation of density fluctuations may be precursors of crystallization. A quantitative analysis was carried out on SAXS patterns (during the induction period) to reveal the nature of these fluctuations.

Observation of a Thermally Driven BCC-FCC Transition in a Block Copolymer Gel using Small-angle X-ray and Neutron Scattering.

J.A.Pople[1], I.W.Hamley[1], J.P.A.Fairclough[2], A.J.Ryan[2], B.U.Komanschek[3], A.J.Gleeson[3], G.E.Yu[4] and C.Booth[4]

1 School of Chemistry, University of Leeds
2 Materials Science Centre, UMIST
3 CLRC Daresbury Laboratory
4 Dept of Chemistry, University of Manchester

The phase behaviour of gels of the block copolymer $E_{40}B_{10}$, where E denotes poly(oxyethylene) and B denotes poly(oxybutylene) and the subscripts are the number of repeat units, in 0.2M potassium sulphate solution has been studied as a function of concentration and temperature. The ordered micellar structure was characterized using small-angle X-ray scattering with simultaneous rheology and small-angle neutron scattering on samples sheared in a Couette cell. The modification of a commercial rheometer for simultaneous synchrotron SAXS experiments is described. For all gel concentrations studied, in the range 25-38wt%, a transition from a BCC micellar phase to an FCC micellar phase was observed on heating, with a further transition to a hexagonal micellar phase at high temperatures. These observations are rationalised on the basis of reduced solvent penetration of the micellar corona with increasing temperature.

CCP13 Travelling Fellowships

CCP13 Travelling Fellowships (£500) are intended to supplement awards to younger UK researchers travelling abroad for a conference involving fibre diffraction in order to give them the opportunity to visit a few fibre diffraction laboratories in the host Country. The £500 is intended to cover the extra travel, accommodation and subsistence costs in the host country involved in visiting these laboratories. It is not intended to cover the basic cost of attending the main conference. The recipients will be asked to report on their visits in a talk to the May Annual Meeting of CCP13 and also to contribute a short (1 page) report for the annual "Fibre Diffraction Review". Current PhD students must have their application countersigned by their research supervisor if they wish it to be considered. Two awards will be made each year.

Application deadline for travel in Summer 1998: APRIL 30th, 1998

Application forms can be obtained from the CCP13 secretary, Dr. G. Mant (g.r.mant@dl.ac.uk).

If awarded, the scholarship will be sent by cheque, once the travel arrangements of the Fellow have been confirmed.

CCP13 Visiting Scientist Fellowship Programme

From time to time the CCP13 Committee will invite an outstanding scientist from overseas to take part in the May Annual CCP13/NCD Workshop and, before or after the Workshop, to visit various contributing laboratories in the UK over a period of one or two weeks to talk to and advise on fibre diffraction methods and results.

CCP13 members are welcome to put forward to the Committee the names and addresses of possible visitors, preferably with some details in writing, including suggestions about which UK scientists/laboratories should be visited.

Forthcoming Meetings

The 7th Annual CCP13/NCD Workshop "Diffraction from Fibres and Polymers"

12 - 14th May 1998

at

CLRC Daresbury Laboratory

For further details please contact The Conference Office, Daresbury Laboratory, Warrington, Cheshire, WA4 4AD.
Tel: 01925 603235.
Fax: 01925 603195
Email: conference@dl.ac.uk
WWW: http://www.dl.ac.uk/SRS/CCP13/workshop98

CENTRAL LABORATORY OF THE
RESEARCH COUNCILS

Produced by
CLRC
Daresbury Laboratory
for CCP13

Useful World Wide Web addresses (URL)

CCP13 Home Page	http://www.dl.ac.uk/SRS/CCP13
NCD Home Page	http://www.dl.ac.uk/SRS/NCD
SRS Home Page	http://www.dl.ac.uk/SRS